

ประสิทธิภาพทางไฟฟ้าของระบบเซลล์เชื้อเพลิงแบบออกไซด์ของแข็งที่ป้อนเชื้อเพลิงด้วย
เอทานอล: การเปรียบเทียบระหว่างกระบวนการกลั่นและเพอร์แอมพอเรชันในการทำ
เอทานอลชีวภาพให้บริสุทธิ์



นางสาวอิสสรာ เชิดเกียรติสกุล

ศูนย์วิทยพัทยากร
จุฬาลงกรณ์มหาวิทยาลัย

วิทยานิพนธ์นี้เป็นส่วนหนึ่งของการศึกษาตามหลักสูตรปริญญาวิศวกรรมศาสตรมหาบัณฑิต


สาขาวิชาวิศวกรรมเคมี ภาควิชาวิศวกรรมเคมี

คณะวิศวกรรมศาสตร์ จุฬาลงกรณ์มหาวิทยาลัย

ปีการศึกษา 2552

ลิขสิทธิ์ของจุฬาลงกรณ์มหาวิทยาลัย

**ELECTRICAL EFFICIENCY OF ETHANOL FUELLED SOLID OXIDE FUEL CELL SYSTEM:
COMPARISON BETWEEN DISTILLATION AND PERVAPORATION FOR BIOETHANOL
PURIFICATION**



Miss Issara Choedkiatsakul

ศูนย์วิทยทรัพยากร
จุฬาลงกรณ์มหาวิทยาลัย
A Thesis Submitted in Partial Fulfillment of the Requirements
for the Degree of Master of Engineering Program in Chemical Engineering

Department of Chemical Engineering

Faculty of Engineering

Chulalongkorn University

Academic Year 2009

Copyright of Chulalongkorn University

520391

ฉัตรภา เวทีเกียรติสกุล : ประสิทธิภาพทางไฟฟ้าของระบบเซลล์เชื้อเพลิงแบบ
ออกไซด์ของแข็งที่ป้อนเชื้อเพลิงด้วยเอทานอล: การเปรียบเทียบระหว่างกระบวนการ
กลั่นและเพอร์แควพอเรชันในการทำเอทานอลชีวภาพให้บริสุทธิ์. (ELECTRICAL
EFFICIENCY OF ETHANOL FUELLED SOLID OXIDE FUEL CELL SYSTEM:
COMPARISON BETWEEN DISTILLATION AND PERVAPORATION FOR
BIOETHANOL PURIFICATION) อ. ที่ปรึกษาวิทยานิพนธ์หลัก: ศ.ดร.สุทธิชัย
อัสตะบำรุงรัตน์, อ. ที่ปรึกษาวิทยานิพนธ์ร่วม: ดร.สุมิตรา จรสโรจน์กุล, 74หน้า.

งานวิจัยนี้ศึกษาและเปรียบเทียบประสิทธิภาพทางไฟฟ้าของระบบเซลล์เชื้อเพลิง
แบบออกไซด์ของแข็งซึ่งรวมเข้าด้วยกันกับกระบวนการทำเอทานอลชีวภาพให้บริสุทธิ์ที่
แตกต่างกันสองวิธีคือ กระบวนการกลั่นและเพอร์แควพอเรชัน จากการศึกษาพบว่าการทำ
เอทานอลชีวภาพให้บริสุทธิ์ด้วยกระบวนการเพอร์แควพอเรชันจะใช้พลังงานความร้อนน้อย
กว่าแต่ต้องการพลังงานไฟฟ้าที่เพิ่มขึ้นสำหรับการทำงานของปั๊มสุญญากาศ นอกจากนี้เมื่อ
ลดความดันของสารในสายเพอร์มิเอทจาก 0.1 บรรยากาศ ลงเหลือ 0.05 บรรยากาศ พบว่า
กระบวนการเพอร์แควพอเรชันจะใช้พลังงานความร้อนน้อยลงในขณะที่พลังงานไฟฟ้าที่
ต้องการกลับเพิ่มมากขึ้น สำหรับการศึกษาหาสภาวะการดำเนินงานที่เหมาะสมของเซลล์
เชื้อเพลิงในระบบเซลล์เชื้อเพลิงแบบออกไซด์ของแข็งซึ่งรวมเข้าด้วยกันกับกระบวนการทำเอ
ทานอลชีวภาพให้บริสุทธิ์นั้นจะดำเนินการ ณ สภาวะที่พลังงานความร้อนสุทธิมีค่าเท่ากับ
ศูนย์ โดยพบว่าสภาวะการดำเนินงานที่เหมาะสมของเซลล์เชื้อเพลิงคือ ใช้ค่าความต่างศักย์
0.65 ถึง 0.80 โวลต์ อุณหภูมิของเซลล์เชื้อเพลิง 973 ถึง 1173 เคลวิน และอัตราส่วนการ
นำกลับเอทานอลมีค่าเป็น 95% และ 99% สำหรับระบบที่รวมเข้าด้วยกันกับกระบวนการกลั่น
และเพอร์แควพอเรชันตามลำดับ ผลการศึกษาพบว่าการรวมระบบการผลิตพลังงานไฟฟ้า
จากเซลล์เชื้อเพลิงเข้าด้วยกันกับกระบวนการเพอร์แควพอเรชัน ณ สภาวะที่ความดันของสาร
ในสายเพอร์มิเอทมีค่าเป็น 0.1 บรรยากาศ จะให้ค่าประสิทธิภาพทางไฟฟ้าสูงที่สุดคือ 41.6%
(ความต่างศักย์ = 0.7 โวลต์, อุณหภูมิ 1173 เคลวิน ค่าการแยกของเมมเบรน 923 และ
อัตราส่วนการนำกลับเอทานอล = 99%)

ภาควิชา...วิศวกรรมเคมี.....ลายมือชื่อนิสิต.....ฉัตรภา เวทีเกียรติสกุล.....
สาขาวิชา...วิศวกรรมเคมี.....ลายมือชื่อ อ.ที่ปรึกษาวิทยานิพนธ์หลัก.....
ปีการศึกษา...2552.....ลายมือชื่อ อ.ที่ปรึกษาวิทยานิพนธ์ร่วม.....

#5170662421 : MAJOR CHEMICAL ENGINEERING

KEYWORDS : SOLID OXIDE FUEL CELL / BIOETHANOL / SIMULATION

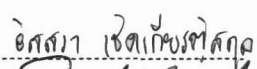
ISSARA CHOEDKIATSAKUL: ELECTRICAL EFFICIENCY OF ETHANOL FUELLED SOLID OXIDE FUEL CELL SYSTEM: COMPARISON BETWEEN DISTILLATION AND PERVAPORATION FOR BIOETHANOL PURIFICATION. THESIS ADVISOR: PROF. SUTTICHAJ ASSABUMRUNGRAT, Ph.D., THESIS CO-ADVISOR: SUMITTRA CHAROJROCHKUL, Ph.D., 74pp.

The overall electrical efficiencies of the solid oxide fuel cell (SOFC) system integrated with two different bio-ethanol purification processes, i.e. distillation and pervaporation were investigated and compared. It was found that the purification by pervaporation consumed less heat energy than that by distillation but the additional electrical power is required for the vacuum pump operation. In addition, two different levels of the permeate pressure for pervaporation were studied. The results show that the lowering pressure at the permeate side from 0.1 atm to 0.05 atm required less heat consumption but more electrical power consumption. For the SOFC system integrated with the purification process, the simulation studies were based on the condition that the net useful heat (Q_{net}) is equal to zero. It was found that the most suitable operating voltage is between 0.65 and 0.8 V and the operating temperature is in the range between 973 and 1173 K. For the effect of the ethanol recovery, the optimal ethanol recovery of the SOFC system integrated with distillation and pervaporation process are 95% and 99% respectively. The results indicate that the SOFC system integrated with pervaporation process with the permeate pressure of 0.1 atm offers the maximum overall electrical efficiency that is 41.6% (voltage = 0.7 V, temperature = 1073 K, separation factor = 923 and ethanol recovery = 99%).

Department : Chemical Engineering

Field of Study : Chemical Engineering

Academic Year : 2009

Student's Signature 

Advisor's Signature 

Co-Advisor's Signature 

ACKNOWLEDGEMENTS

The author would like to show high appreciation to Professor Suttichai Assabumrungrat for his great guidance in both research study and life attitude during the author's research study and Dr.Sumittra Charojrochkul for her good advice and kind assistance. In addition, the author wishes to thank Dr.Waret Veerasai for providing her support and facilities in the lab at Mahidol University. Special thank to Associate Professor Muenduen Phisalaphong as the chairman, Associate Professor ML. Supakanok Tongyai and Assistant Professor Worapon Kiatkittipong as the members of the thesis committee.

Many thanks National Metal and Materials Technology Center (MTEC), Thailand for providing her financial supports and great opportunity during her Master degree.

The author would like to gratefully thank members in Center of Excellence on Catalysis and Catalytic Reaction Engineering, Department of Chemical Engineering, Faculty of Engineering, Chulalongkorn University who have assisted her over the years of her study.

Finally, the author would like to express great gratitude to her parents, sisters and brother. The author cannot completely achieve a success in her study without the support from her family.

CONTENTS

	page
ABSTRACT (THAI).....	iv
ABSTRACT (ENGLISH).....	v
ACKNOWLEDGEMENTS.....	vi
CONTENTS.....	vii
LIST OF TABLES.....	x
LIST OF FIGURES.....	xi
NOMENCLATURES.....	xiii
CHAPTERS	
I INTRODUCTION.....	1
II THEORY.....	3
2.1 Fuel Cell Principles.....	3
2.1.1 Basic Principles.....	3
2.1.2 Fuel cell Components.....	4
2.1.3 Types of Fuel Cells.....	4
2.1.4 Fuel Cell Advantages and Disadvantages.....	6
2.2 Solid Oxide Fuel Cell.....	7
2.2.1 Operating Principles.....	7
2.2.2 Reforming Process.....	9
2.2.3 Characteristics of SOFCs.....	10
2.3 Ethanol Steam Reforming Reaction.....	12
2.4 Pervaporation Process.....	14
2.4.1 Basic Principles.....	14
2.4.2 Characterization of Membrane.....	15
2.4.3 Membrane for Ethanol Recovery.....	17
2.4.4 Applications of Pervaporation.....	19
III LITERATURE REVIEW.....	21
3.1 Fuels Used in SOFC and the optimal Operating Conditions.....	21
3.2 Distillation Process Integrated with the SOFC System.....	24

CHAPTERS	page
3.3 Membrane for Ethanol/Water Separation in Pervaporation.....	25
3.4 SOFC modeling.	27
IV MODELLING.....	30
4.1 Bioethanol Purification Process.....	30
4.1.1 Distillation Process.....	30
4.1.2 Pervaporation Process.....	31
4.2 SOFC System Modelling	34
4.2.1 Electrochemical Model.....	36
4.2.2 Calculation Procedures.....	41
V RESULTS AND DISCUSSIONS.....	44
5.1 The optimal Operating Conditions for Bioethanol Purification.....	44
5.1.1 Distillation.....	44
5.1.2 Pervaporation.....	46
5.1.3 Comparison between Distillation and Pervaporation.....	49
5.2 Performance of the SOFC System at the Base Condition.....	50
5.2.1 Effect of Operating Voltage.....	50
5.2.2 Effect of Operating Temperature.....	52
5.2.3 Effect of Ethanol Recovery.....	54
5.3 Performance of the SOFC System Integrated with Two Different Purification Processes.....	55
5.3.1 Performance at the Base Conditions.....	55
5.3.2 The appropriate Operating Conditions for the SOFC System Integrated with the Purification Process ($Q_{net} = 0$).....	59
VI CONCLUSIONS AND RECOMMENDATIONS.....	63
6.1 Conclusions.....	63
6.2 Recommendations.....	64
REFERENCES.....	65
APPENDICES.....	69

CHAPTERS	page
APPENDIX A.....	70
APPENDIX B.....	71
APPENDIX C.....	73
VITAE.....	74



ศูนย์วิทยทรัพยากร
จุฬาลงกรณ์มหาวิทยาลัย

LIST OF TABLES

Table		Page
2.1	Summary of fuel cell types and their present characteristics.....	5
2.2	Membranes used for ethanol recovery in pervaporation process and its performance.....	18
2.3	The alcohol/water separation factors reported in the literature for silicalite-PDMS mixed matrix membranes.....	19
4.1	Summary of model parameters.....	41
5.1	The total heat consumption and the optimal operating conditions for bioethanol purification by distillation process.....	46
5.2	The total heat and electrical power consumption and the optimal operating conditions for bioethanol purification by pervaporation process (25 mol% of ethanol).....	49
5.3	The total heat and electrical power consumption comparison between distillation and pervaporation process.....	50
A1	Heat capacities of various components (C_p).....	70
A2	Heat of formation (H_f^0) and entropy (S^0) of various components at standard state (298 K, 1 atm).....	70

ศูนย์วิทยทรัพยากร
จุฬาลงกรณ์มหาวิทยาลัย

LIST OF FIGURES

Figure		Page
2.1	The schematic diagram of fuel cell.....	3
2.2	Basic principle of SOFC operation (a) SOFC-H ⁺ (b) SOFC-O ²⁻	8
2.3	The configurations of SOFC modes (a) ER-SOFC (b) IIR-SOFC (c) DIR-SOFC.....	10
2.4	The schematic diagram for pervaporation process.....	14
4.1	The schematic diagram of purification process by distillation.....	31
4.2	The schematic diagram of purification process by pervaporation.....	32
4.3	The involved variables for mass balance equation.....	33
4.4	The schematic diagram of the SOFC system.....	35
4.5	The SOFC stack area separation for the calculation.....	41
4.6	The flow chart of the program calculation procedures.....	43
5.1	Effect of ethanol purity on the heat consumption (Q) for distillation column (Ethanol recovery = 90%).....	45
5.2	Effect of the ethanol purity on the total heat consumption (Q _{net}) for distillation column (Ethanol recovery = 90%).....	45
5.3	Effect of the separation factor on the ethanol purity at permeate stream and the permeate flow rate.....	47
5.4	Effect of the separation factor on the total heat (Q _{total}) and electrical power consumption (W _e) (Permeate pressure = 0.1 atm).....	48
5.5	Effect of operating voltage and fuel utilization on (a) the power density and the area of SOFC stack and (b) the electrical efficiency and the net useful heat (Q _{net}) (Ethanol recovery = 80%, Temperature = 1073 K).	51
5.6	Effect of the operating temperature and fuel utilization on (a) the power density and the area of SOFC stack and (b) the overall electrical efficiency and heat of the SOFC stack (Q _{SOFC}) (Ethanol recovery = 80%, Voltage = 0.7 V).....	53

Figure		Page
5.7	Effect of the ethanol recovery and fuel utilization on the overall electrical efficiency and the net useful heat (Q_{net}) (Ethanol recovery = 80%, Voltage = 0.7 V, Temperature = 1073 K).....	54
5.8	Energy and temperature for various units in SOFC system integrated with distillation process (Ethanol recovery = 80%, Voltage = 0.7 V, $C_{EtOH, distillate} = 40$ mol%, Fuel utilization = 70%).....	56
5.9	Energy and temperature for various units in SOFC system integrated with pervaporation process (Ethanol recovery = 80%, Voltage = 0.7 V, $C_{EtOH, permeate} = 25.7$ mol%, Separation factor = 49, Fuel utilization = 70%, Permeate pressure = 0.1 atm).....	56
5.10	Effect of operating voltage on the net useful heat in distillation and pervaporation process at the base condition (Fuel utilization = 70%).....	57
5.11	Effect of operating voltage on the net useful heat in distillation and pervaporation process at the base condition (Fuel utilization = 80%)....	58
5.12	Effect of operating voltage on the net useful heat in distillation and pervaporation process at the base condition (Fuel utilization = 90%)....	58
5.13	Effect of the operating voltage on (a) the heat of SOFC stack (Q_{SOFC}) and the area of SOFC stack and (b) the power density and the area of SOFC stack (Ethanol recovery = 80%, Temperature = 1073 K).....	60
5.14	Effect of the operating temperature on (a) the heat of SOFC stack (Q_{SOFC}) and the area of SOFC stack and (b) the power density and the area of SOFC stack (Ethanol recovery = 80%, Voltage = 0.7 V).....	61
5.15	Effect of the ethanol recovery on the overall electrical efficiency and the area of SOFC stack (Voltage = 0.7 V, Temperature = 1073).....	62

NOMENCLATURES

A	cell stack area	$[m^2]$
C_i	concentration of species i	$[\text{mol } \%]$
C_p	heat capacity	$[\text{kJ kmol}^{-1} \text{K}^{-1}]$
D	carbonator bed diameter	$[m]$
$D_{i,K}$	Knudsen diffusivity of component i	$[\text{cm}^2 \text{s}^{-1}]$
D_{A-B}	ordinary diffusivity of gas A versus gas B	$[\text{cm}^2 \text{s}^{-1}]$
$D_{i(\text{eff})}$	effective diffusion coefficient of electrode i	$[\text{cm}^2 \text{s}^{-1}]$
$D_{i,k(\text{eff})}$	effective Knudsen diffusivity of component i	$[\text{cm}^2 \text{s}^{-1}]$
$D_{A-B(\text{eff})}$	effective ordinary diffusivity of gas A versus gas B	$[\text{cm}^2 \text{s}^{-1}]$
E	theoretical open-circuit voltage of the cell	$[V]$
E_0	theoretical open-circuit voltage of the cell at standard pressure	$[V]$
E_a	activation energy	$[\text{kJ mol}^{-1}]$
F	Faraday constant (9.6495×10^4)	$[\text{C mol}^{-1}]$
i	current density	$[\text{A cm}^{-2}]$

i_0	exchange current density	[A cm ⁻²]
i_{ave}	average current density	[A cm ⁻²]
J_i	Permeate flux of species i	[mol m ⁻² s]
l	membrane thickness	[m]
l_a	thickness of anode electrode	[μm]
l_c	thickness of cathode electrode	[μm]
l_e	thickness of electrolyte	[μm]
LHV_i	lower heating value of component i	[kJ kmol ⁻¹]
m	molar flow rate	[mol s ⁻¹]
M_i	molecular weight of gas i	[g]
n	electrode porosity	[-]
n_i	molar flow rate of component i	[mol s ⁻¹]
p_{ave}	average power density	[W cm ⁻²]
p_i	partial pressure of component i	[Pa]
p_i^i	inlet pressure of component i	[Pa]
P	pressure	[Pa]
P_{ref}	reference pressure (10 ⁵)	[Pa]

Q	heat energy	[MW]
Q_{net}	net useful heat	[MW]
Q_{stack}	heat of an SOFC stack	[MW]
R	gas constant (8.3145)	[J mol ⁻¹ K ⁻¹]
T	temperature	[K]
U_f	fuel utilization	[-]
V	cell voltage	[V]
W_e	electrical power	[MW]
$W_{e,net}$	net electrical power	[MW]
W_{pump}	electrical power consumed in pump	[MW]
x_i	mole fraction of component i at retentate side of the membrane	[-]
y_i	mole fraction of component i at permeate side of the membrane	[-]
z	number of electron participating in the electrochemical reaction	[-]

Greek letters

α	charge transfer coefficient	[-]
ξ	electrode tortuosity	[-]
δ_{O_2}	coefficient used in concentration overpotential	[-]
η_{act}	activation loss	[V]
η_{conc}	concentration loss	[V]
η_{ohm}	ohmic loss	[V]
η_{pump}	pump efficiency	[-]
σ_{AB}	collision diameter	[Å]
Ω_D	collision integral	[-]
ε_{AB}	Lennard-Jones energy interaction parameter scaled with respect to the Boltzman constant	[-]
γ_a	pre-exponential factor for anode exchange current Density	[A m ⁻²]
γ_c	pre-exponential factor for cathode exchange current Density	[A m ⁻²]

Subscripts

a anode

c cathode



ศูนย์วิทยทรัพยากร
จุฬาลงกรณ์มหาวิทยาลัย

CHAPTER I

INTRODUCTION

The demand for energy is continuously increasing due to the growth of the world population and the development in modern technologies. However, the sources of energy are limited and going to be shortage in the near future. Therefore, the renewable and clean energy is an urgent and crucial issue. Solid oxide fuel cell (SOFC) is one of promising technologies. It can convert chemical energy of a fuel directly to electricity with high efficiency and, therefore, is considered as a clean energy generator which reduces green house gas emission to environment. In addition, fuel flexibility is the greatest advantage of SOFC as compared to other types of fuel cell.

Various fuels can be fed to SOFC, such as ammonia, methane, biogas, methanol, ethanol, etc. Ammonia can be used as the fuel for SOFC because it can decompose into hydrogen and nitrogen. Therefore, it is a good hydrogen carrier and is carbon-free (Zhang and Yang, 2008). However the major energy carrier in the nature is hydrocarbons so we can not evade to using these fuels. Methane might be an alternative fuel that can be used because it is the simplest hydrocarbon fuel. It has a lower probability for coking which is one of the important problems in fuel cell (Hao and Goodwin, 2008). Moreover biogas can also be used because it mainly contains methane and carbon monoxide (Shiratori et al., 2008) but it has a major problem about the deposition of carbon on the catalyst. Methanol have been used in many researches because of many good reasons such as ease of handling, transportation and storage, clear and renewable source that can be derived from all fossil resource, agricultural byproducts and biomass (Liu et al., 2008).

Nowadays biomass-derived fuel has attracted considerable attention. Bioethanol is one of the promising renewable fuels for fuel cells. It is non-toxic and easy for storage

and transportation. In order to operate the SOFC, bioethanol is first purified to a desired ethanol concentration and then converted to hydrogen-rich gas before being fed into the SOFC system.

There are a number of possible choices for bioethanol purification processes. The most widely used is the conventional distillation. Wassana Jamsak et al. (2007) reported that a solid oxide fuel cell integrated with a distillation column can be operated without demanding an additional heat source. Pervaporation is one of the interesting technologies for bioethanol purification. Since it is independent on the vapor/liquid equilibrium but only depends on the difference in transportation rate of individual components through a membrane. Moreover, there are a number of research focusing on improvement of membrane for alcohol separation.

According to the reasons mentioned above, this research was, hence, focused on the performance analysis of solid oxide fuel cell system fuelled by bioethanol for electricity generation. The performance includes power density, area of SOFC stack, total SOFC stack heat generation and electrical efficiency. In addition, the effects of operating parameters for both the SOFC system and the purification processes were also studied. Particular interest is on the comparison of SOFC system performance between two different bioethanol purification processes; i.e. 1) conventional distillation and 2) pervaporation. The best system can be selected by comparing the highest electrical efficiencies achievable from the two systems with different bioethanol purification processes.

CHAPTER II

THEORY

2.1 Fuel Cell Principle

2.1.1 Basic Principle

A fuel cell is an electrochemical conversion device that relies upon a continuous feed of a fuel to produce DC electricity and, as by-products, heat and water. Fuel cells are unique in terms of the variety of their potential applications; it can provide energy for systems as large as a utility power station and as small as a laptop computer. A cell contains an anode, a cathode and an electrolyte layer, with a typical system being shown in Figure 2.1. The electrolyte allows the passage of the ions, whilst the negatively charged electrons pass around an external circuit, thus creating an electric current. At the interface with the electrodes, the reactions take place during which water and heat is produced.

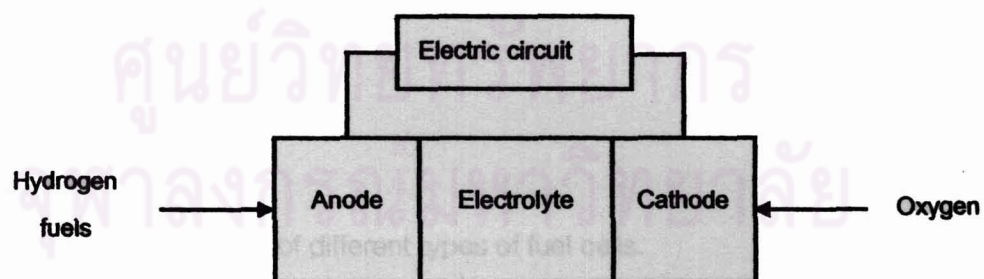


Figure 2.1 The schematic diagram of fuel cell

2.1.2 Fuel Cell Components

2.1.2.1 Electrolyte

The electrolyte is a material that allows the passage of the ions from one electrode to the other. The electrolyte material is high ion conductivity, less electrical conductivity and thermal stability. The specific type of material depends on the type of fuel cell.

2.1.2.2 Anode

The anode of state-of-the-art SOFCs is a cermet made of metallic nickel and a YSZ skeleton. The anode has a high porosity (20–40%) so that mass transport of reactant and product gases is not inhibited.

2.1.2.3 Cathode

Similar to the anode, the cathode is a porous structure that must allow rapid mass transport of reactant and product gases. Strontium-doped lanthanum manganite ($\text{La}_{0.84}\text{Sr}_{0.16}\text{MnO}_3$), a p-type semiconductor, is most commonly used for the cathode material.

Apart from these base components, the fuel cell also contains current collectors, interconnects and manifolds.

2.1.3 Types of Fuel Cells

There are a number of different types of fuel cells.

- Alkaline fuel cells (AFCs)
- Direct methanol fuel cells (DMFCs)
- Molten carbonate fuel cells (MCFCs)
- Phosphoric acid fuel cells (PAFCs)

- Proton-exchange membrane fuel cells (PEMFCs)
- Solid oxide fuel cells (SOFCs).

Apart from DMFC, which is technically a subset of the polymer electrolyte membrane fuel cells, others are named after their electrolyte type. Table 2.1 shows the summary of fuel cell types and their present characteristics.

Table 2.1 Summary of fuel cell types and their present characteristics (Appleby and Foulkes, 1993)

Fuel cell type	Operating temp. (°C)	Applications	Electrical power range (kW)	Overall Electrical efficiency (%)
PEMFCs	60–110	Mobile, portable, low power generation	0.01–250	40–55
AFCs	70–130	Space, military, mobile	0.1–50	50–70
DMFCs	60–120	Portable, mobile	0.001–100	40
PAFCs	175–210	Medium- to large-scale power and CHP	50–1,000	40–45
MCFCs	550–650	Large-scale power generation	200–100,000	50–60
SOFCs	500–1,000	Medium- to large-scale power and CHP, vehicle auxiliary power units, off-grid power and micro-CHP	0.5–2,000	40–72

2.1.4 Fuel Cell Advantages and Disadvantages

Obviously, fuel cells have various advantages compared to conventional power sources, such as internal combustion engines or batteries. Although some of the fuel cells' attributes are only valid for some applications, most advantages are more general. However, there are some disadvantages facing developers and the commercialization of fuel cells as well.

2.1.4.1 Advantages

- Fuel cells eliminate the pollution caused by burning fossil fuels; the only byproduct is water.
- If the hydrogen that use for the fuel cell comes from the electrolysis of water, then using fuel cells eliminates greenhouse gases.
- Fuel cells do not need conventional fuels such as oil or gas. Therefore, it can eliminate the economic dependence on those fuels.
- The production of potential fuel which is hydrogen can be distributed.
- The efficiency of fuel cell is higher than that of the diesel or gas engines.
- The operation is silently compared to internal combustion engines
- The operating times are much longer than with batteries, since doubling the operating time needs only doubling the amount of fuel which does not depend on the capacity of the unit.
- The maintenance of fuel cells is simple since there are few moving parts in the system.

2.1.4.2 Disadvantages

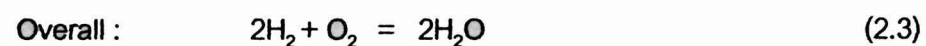
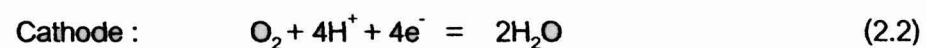
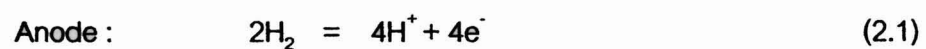
- Fuelling fuel cells is still a problem since the production, transportation, distribution and storage of hydrogen is difficult.
- Reforming hydrocarbons via reformer to produce hydrogen is technically challenging and not clearly environmentally friendly.
- The refueling and the starting time of fuel cell vehicles are longer than in a "normal" car.
- Generally, fuel cells are slightly bigger than comparable batteries or engines. However, the size of the units is decreasing.
- The production of fuel cell is expensive.
- The technology is not fully developed and few products are available.

2.2 Solid Oxide Fuel Cell

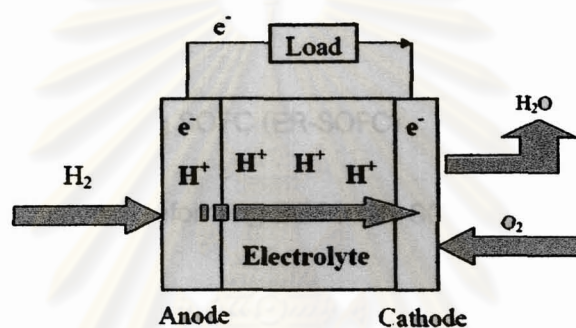
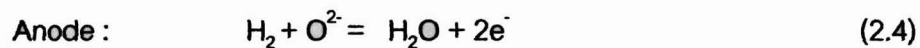
2.2.1 Operating Principle

There are two types of electrolytes which are possible for SOFC operation; namely, a proton conducting electrolyte and an oxygen ion conducting electrolyte. Because of the difference in type of mobile ion, the reactions occurring at the electrodes are also different as shown in Figure 2.2

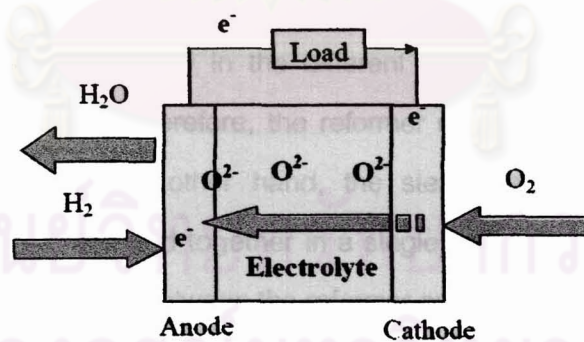
The electrochemical reaction in the SOFC-H⁺



The electrochemical reaction in the SOFC-O²⁻



(a)



(b)

Figure 2.2 Basic principle of SOFC operation (a) SOFC-H⁺ (b) SOFC-O²⁻

In the case of SOFC-H⁺, hydrogen molecules at the anode separate into proton ions and electrons. The proton ions move across the electrolyte and react with oxygen

molecules at the cathode. The steam is then produced at the cathode. In contrast, for the SOFC- O^2 , the species that pass through the electrolyte is oxygen ion which generate from the oxygen molecules at the cathode gain electrons from the current circuit. The oxygen ion is then reacted with the hydrogen molecules at the anode and the electrochemical reaction takes place generating the steam.

2.2.2 Reforming Process

When SOFCs are operated with a fuel, such as hydrocarbon and alcohol, three modes of operation are possible.

- External reforming SOFC (ER-SOFC)
- Indirect internal reforming SOFC (IIR-SOFC)
- Direct internal reforming SOFC (DIR-SOFC)

The configurations of three modes are shown in Figure 2.3.

For ER-SOFC operation, the steam reforming reactions and the electrochemical reactions are operated separately in the different units and there is no direct heat transfer between both units. Therefore, the reformer unit requires high energy for the endothermic reaction. On the other hand, the steam reforming reaction and the exothermic reaction are operated together in a single unit for both IIR-SOFC and DIR-SOFC. Therefore, heat transfer between the reformer and SOFC is available.

For IIR-SOFC, the reforming reaction occurs nearby the cell stack then the heat transfer from the fuel cell chamber to the reformer is available. However, there is only some part of heat can be utilized since the heat transfer rate is limited. In case of DIR operation, the reforming reaction takes place at the anode of the fuel cell. Heat and steam released from the electrochemical reaction is effectively used for the endothermic reforming reaction since both processes take place simultaneously at the anode. Therefore, in term of energy aspect, DIR-SOFC is more attractive than the others.

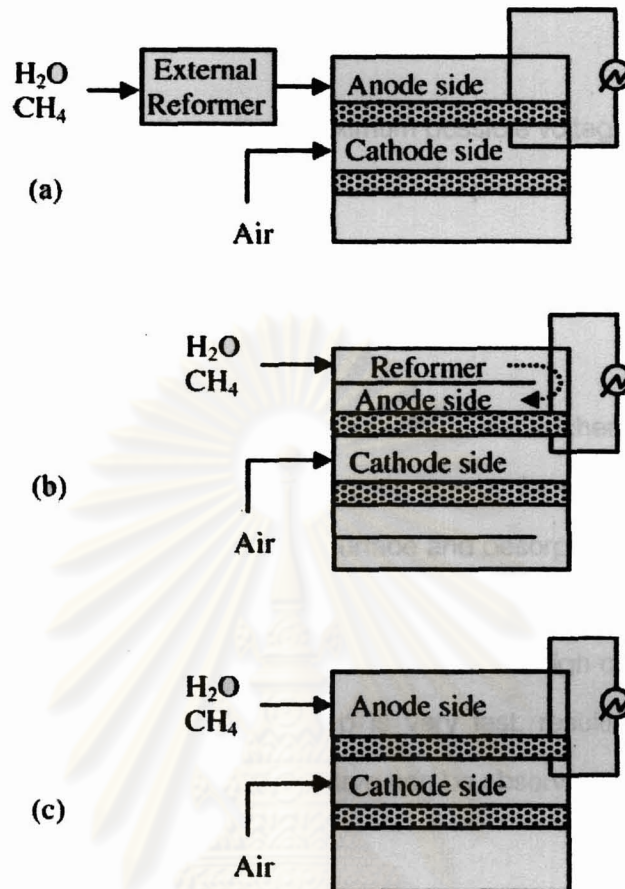


Figure 2.3 The configurations of SOFC modes (a) ER-SOFC (b) IIR-SOFC (c) DIR-SOFC

2.2.3 Characteristics of SOFCs

2.2.3.1 Open circuit voltage

Open circuit voltage (OCV) is the maximum possible voltage that can be achieved when operating at a specific condition. Due to different concentration of components between the anode and the cathode, this causes different potential at the anode and cathode and results in OCV of the cell. OCV drives electrons from one electrode to another and generates current.

2.2.3.2 Losses

Though the OCV is the theoretical maximum possible voltage, the actual voltage of SOFC is always less than the theoretical value due to presence of losses. Losses can be divided into four types.

a) Activation Loss

Activation loss is the loss which occurs from electrochemical reaction at the electrodes. Some energy is required as activation energy for electrochemical reaction, e.g. adsorption of reactant on the electrode surface and desorption of product out of the surface. Generally, activation loss dominates at low current density and the characteristics curve also exhibit non-linear. However, at the high operating temperature like SOFC temperature, the rate of this step is very fast, resulting in small value of activation losses. The linear characteristics curve can be observed.

b) Ohmic Loss

Ohmic loss is a major loss in the SOFC stack when compared to other losses. Ohmic loss results from the resistance of flow of electrons through the electrodes and an interconnector and the resistance of flow of ion passing through an electrolyte.

c) Fuel Crossover or Internal Current Loss

Normally, an electrolyte should transport only ions through the cell and no fuel cross over the electrolyte. However, fuel crossing through an electrolyte or electrons leaking to an electrolyte is possible. Generally, fuel crossover loss is very small.

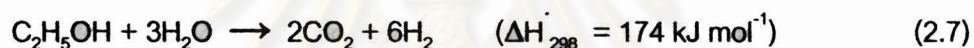
d) Concentration Loss

Concentration loss is caused by the large reduction in concentration of fuel or oxidant when operating SOFC at high current density or high fuel utilization. The difference between the concentration of gas in the bulk and the concentration of gas on

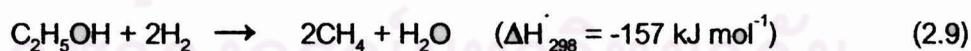
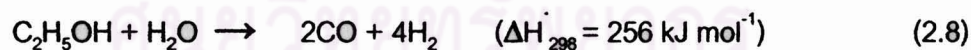
the electrode surface causes this type of loss. At lower fuel utilization and current density, concentration loss is very small.

2.3 Ethanol Steam Reforming Reaction

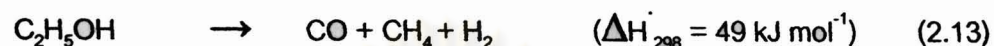
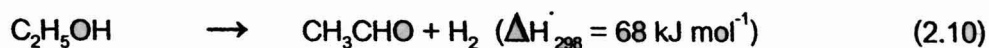
Thermodynamic aspects of ethanol steam reforming have received a fair amount of attention in the published literature. The reaction is strongly endothermic and produces only H₂ and CO₂ if ethanol reacts in the most desirable way. The basic reaction scheme is as follows:



However, other undesirable products such as CO and CH₄ are also usually formed during the reaction. Aupretre et al. (2005) have discussed the main reactions in ethanol steam reforming that account for the formation of these by-products:

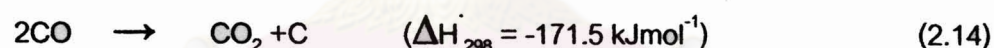


Other reactions that can also occur are: ethanol dehydrogenation to acetaldehyde (2.10), ethanol dehydration to ethylene (2.11), ethanol decomposition to CO₂ and CH₄ (2.12) or CO, CH₄ and H₂ (2.13).



Acetaldehyde and ethylene are important intermediates that may be formed during reaction even at relatively low temperatures well before the formation of H_2 and CO_x by reactions (2.7) and (2.8).

In addition, the formation of coke on the surface of the catalyst is also not uncommon. Coke formation may occur as per the following Boudouard reaction:



Another possible route for the formation of carbon is through ethylene:



From the thermodynamic standpoint, since reaction (2.7) is endothermic and results in increase in number of moles, increasing the temperature and lowering the pressure is in favor of ethanol reforming.

The water gas shift reaction (2.16) always takes place due to the presence of CO.



2.4 Pervaporation Process

2.4.1 Basic Principle

The pervaporation process to separate liquid mixtures is shown schematically in Figure 2.4. A feed liquid mixture contacts one side of the membrane; the permeate stream is removed as a vapor from the other side. Transport through the membrane is induced by the vapor pressure difference between the feed solution and the permeate vapor. This vapor pressure difference can be maintained in several ways. In the laboratory, a vacuum pump is usually used to draw a vacuum on the permeate side of the system.

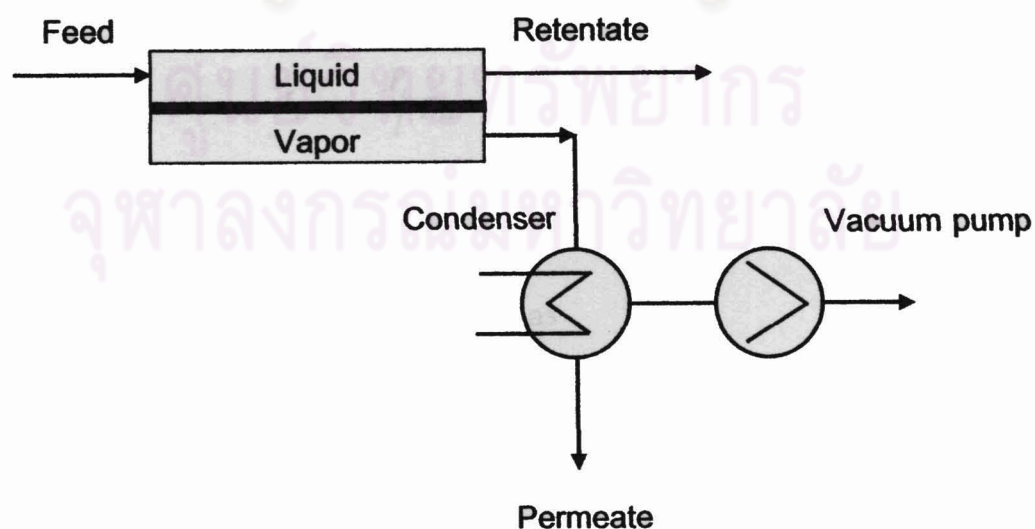


Figure 2.4 The schematic diagram for pervaporation process

2.4.2 Characterization of Membrane

2.4.2.1 Permeability

The phase change of the permeating species is one of the most different features of pervaporation. Based on the solution-diffusion model, the flux equation can be written as:

$$J_i = \frac{P_i}{l}(p_{i0} - p_{i1}) \quad (2.17)$$

where the permeability coefficient of the membrane with respect to the driving force expressed in terms of partial vapor pressure (P_i) is related to the solubility coefficient (S) and the diffusivity coefficient (D) as illustrated in Eq. (2.20)

In the pervaporation process, when the permeate pressure (p_{i1}) is kept as low value, Eq. (2.17) can be expressed as:

$$J_i = \frac{P_i}{l} p_{i0} \quad (2.18)$$

and the permeation rate can be expressed as

$$Q_i = P_i A c_i \quad (2.19)$$

The permeability in Eq. (2.17) – (2.19) is defined as:

$$P_i = D_i S_i \quad (2.20)$$

The temperature dependence can be expressed as Eqs. (2.21) – (2.22), respectively.

$$D_i = D_{i,0} \exp\left(-\frac{E_{a_D}}{RT}\right) \quad (2.21)$$

$$S_i = S_{i,0} \exp\left(-\frac{E_{a_S}}{RT}\right) \quad (2.22)$$

Thus, the permeability can be written as the following equation.

$$P_i = P_{i,0} \exp\left(-\frac{E_{a_P}}{RT}\right) \quad (2.23)$$

2.4.2.2 Membrane separation factor

Membrane separation factor is defined as the ratio of the mole fractions of components A and B in the permeate and feed sides as follow:

$$\alpha_{A/B} = \frac{y_A / y_B}{x_A / x_B} \quad (2.24)$$

2.4.3 Membrane for Ethanol Recovery

Many membrane materials have been studied for the purpose of recovering ethanol from water. Table 2.2 shows some of the membranes that were used for ethanol recovery in the pervaporation process.

Vane (2005) reviewed that the current benchmark hydrophobic pervaporation membrane material is poly(dimethyl siloxane) [PDMS], often referred to as 'silicone rubber' which is an elastomeric material. Much effort has been expended searching for polymeric materials with better ethanol–water separation performance than PDMS. Unfortunately, seldom materials been reported to improve upon PDMS.

While no organic membrane has yet to challenge PDMS as the benchmark hydrophobic pervaporation membrane material, inorganic membranes based on hydrophobic zeolites have shown both higher ethanol–water separation factors and ethanol fluxes than PDMS membranes. Since it is very costly and difficult to manufacture the defect-free commercial-scale silicalite-1 membranes then several groups have investigated the potential of mixed matrix membranes consisting of silicalite-1 particles dispersed in PDMS. The performance of these mixed matrix materials is dependent on the loading of silicalite-1, size of the particles, source of silicalite-1 and membrane casting conditions. The increased performance characteristics with little cost increase have led to the interest in mixed matrix membrane materials. Table 2.3 shows the alcohol–water separation factors reported in the literature for silicalite-PDMS mixed matrix membranes.

Table 2.2 Membranes used for ethanol recovery in pervaporation process and its performance.

Number	Membrane material	Separation factor	Flux (g/m ² h)	Reference	Remark
1	Silicalite-filled PEBA	3.6	833	Gu et al. (2009)	Feed 5 wt %EtOH, 40 °C
2	Silicalite coated with silicone rubber	125	140	Matsuda (2002)	Feed 5 vol%EtOH, add 3 %wt silicone rubber, 30 °C
3	PDMS/PVDF composite membrane	15	450	Zhan et al. (2008)	Feed 5 wt.% ethanol, 60 °C
4	Silicalite-1 membranes	69	870	Chen et al. (2008)	Feed 3 wt% ethanol, No commercial, 60 °C
5	silicone/PVDF	31	900	Chang et al. (2004)	Feed 10 wt.% ethanol, 60 °C
6	PDMS cast on C-A	8.5	1300	Lia et al. (2004)	Feed 5 wt %EtOH, 30 °C
7	PDMS (SolSep 3360)	7	1000	Verhoef et al. (2008)	Feed 10 wt.% ethanol, 44 °C
8	Zeolite–silicone rubber mixed matrix membranes	1.9	110	Vane (2008)	Feed 5 wt %EtOH, 50 °C
9	TOA immobilized in pore of polypropylene hollow fiber membranes	80	1.2	Atsawin Thongsukmak and Sirkar (2007)	Feed 0.5 wt %EtOH, 54 °C
10	PDMS-PAN-PV membrane	> 8	2600 – 3500	Lewandowska et al. (2007)	Feed 4.56 %m/v EtOH, 30 °C

Table 2.3 The alcohol/water separation factors reported in the literature for silicalite-PDMS mixed matrix membranes. (Vane, 2005)

Number	Silicalite Loading (wt %)	Separation factor	Feed Temp. (°C)	Remark (Conc., Flux, Vacuum, thickness)
1	77	59	22	7wt% EtOH, 125 μm , < 1 μm particles
2	77	34	22	5wt% EtOH, 20 μm , < 1 μm particles
3	50	29.3	50	4.4wt% EtOH
4	40	28	40	0.01wt% EtOH in aroma compound
5	70	17	30	5wt% EtOH, 100 μm , 1.8 μm particles
6	60	16.5	22.5	5wt% EtOH, 100 μm , ~5 μm particles
7	62	13-16	22	7wt% EtOH, 4-12 μm , < 1 μm particles
8	30	15.7	35	6wt% EtOH, < 2 torr, nanoscale silicalite
9	40	14.9	22.5	5wt% EtOH, ~100 μm , ~5 μm particles
10	-	11.1	66	1.5wt% EtOH, 10 torr
11	30	~10	35	6wt% EtOH
12	50	7.5	60	4.8wt% EtOH, < 5 μm particles
13	50	~7	35	6wt% EtOH, composite membrane

2.4.4 Applications of Pervaporation

2.4.4.1 Organophilic membranes

Organophilic membranes are mostly applied for the removal of volatile organic components (VOC's) from gas stream like waste air or nitrogen. Although considerable effort in research and development has been devoted to the removal of VOC's from aqueous streams but this technique has not yet been introduced into the industry because the system are more complex and the economical value of the recovered substances is low.

2.4.4.2 Hydrophilic membranes

The largest industrial installations of pervaporation are equipped with hydrophilic membranes and used for the removal of water from organic solvents and solvent mixtures.

- Solvent dehydration

The most important solvents to be treated are the light alcohols, esters, ketones and ethers. The final water concentrations to be reached vary between 1% to below 500 ppm for the alcohols and to below 100 ppm for ethers.

- Removal of water from reaction mixtures

In many chemical reactions like esterification, acetalisation, ketalisation, or etherification water is produced as an unwanted by-product. The equilibrium reaction is of the form:



Removal of the water from the mixture will shift the reaction equilibrium to the side of the wanted product.

- Organic-organic separation

The separations of real organic-organic mixtures have still been to developed and introduced into industrial application. However, specific modification of hydrophilic membranes can be used to remove the light alcohols methanol and ethanol from their mixtures with other organics. The selectivity of these membranes is not that high as in dehydration processes, but sufficient for effective and economical large scale industrial application.

CHAPTER III

LITERATURE REVIEW

The research on SOFC has been carried out extensively. In this chapter, the literature reviews are divided into four main parts. The first part is about the research on the proper fuels and the optimal operating conditions for the SOFC system in order to make the highest performance. The second part reviewed on the study of the distillation process integrated with SOFC system. The third part mentions about the membrane for ethanol/water separation in pervaporation process and the last part is about the research study on the SOFC modeling.

3.1 Fuels Used in SOFC and the optimal Operating Conditions

As a variety of primary fuels can be fuelled to the SOFC system, there are many researches attempting to investigate performance of SOFC systems fed by different fuels. Hydrogen is the main fuel for SOFC. If other fuels are used, it needs to be reformed into hydrogen rich gas before being fed to the fuel cell stacks. In general, the conversion of fuels to hydrogen can be carried out by three main reaction processes namely, steam reforming (SR), partial oxidation (POX) and auto-thermal reforming. Rabenstein and Hacker (2008) investigated the thermodynamic equilibrium of ethanol steam-reforming, partial-oxidation and auto-thermal reforming by Gibbs enthalpy minimization including the possibility of solid coke formation. This research studies the effect of the parameters such as steam-to-ethanol ratio, oxygen-to-ethanol ratio and temperatures to each of reactions. Steam-reforming operation gives a higher hydrogen-yield as in partial-oxidation operation and get low carbon monoxide content in the reformer effluent. So there was no danger of coke formation. In partial-oxidation operation high hydrogen content appears in conjunction with high carbon monoxide

content. From the thermodynamic aspects this is unfavorable choice due to high carbon monoxide content and the need of anhydrous ethanol feed, which is costly in production. In case of auto-thermal reforming, no strong effect on the hydrogen and carbon monoxide formation at temperatures below 873 K and over the whole S/E-ratio range and it can reduce the coke-formation and energy demand for the reforming process. Total energy demand is of the order $POX > ATR > SR$.

Zhang and Yang (2008) investigated the direct ammonia solid oxide fuel cell based on thin proton-conducting electrolyte to avoid the formation of NO_x . At the anode, protons are generated and transported through the proton-conducting electrolyte to the cathode and react with surface oxygen ions generated electrochemical reaction. Only nitrogen and water are the chemical products. The maximum power density was 147 and 200 $mWcm^{-2}$ at 873 and 923 K. When test with hydrogen fuel, the maximum power density was 172 and 223 $mWcm^{-2}$ at 873 and 923 K, respectively indicating that ammonia can be treated as a substitute liquid fuel for SOFCs.

The fuel cell efficiency and fuel utilization of a methane-powered single-chamber solid oxide fuel cell as a function of operating parameters including flow rate, fuel-to-oxygen ratio, fuel cell layout and balance gas was studied by Hao and Goodwin (2008). They found that when using slow flow speed, high efficiency and fuel utilization can be achieved, but the depletion of fuel and oxygen by the upstream portion of the cell is also serious, resulting in a low total power. On the other hand when using fast flow speed, the local power density at the downstream part of the cell increases significantly and the total power is boosted, but the amount of the unspent fuel also increases proportionally with the flow speed, resulting in a low efficiency and fuel utilization. In order to solve this problem they operated the fuel cell under optimum fuel/oxygen ratio and with highly diffusive balance gas including rotating the cell, reducing the gas chamber width or increasing the length of the single cell but the efficiencies are found not as effective. However, the maximum achievable efficiency of a single-cell SC-SOFC is above 10%

and the efficiency at typical operating conditions is above 5% significantly higher than the reported 1% in literature.

Shiratori et al. (2008) researched on the direct feeding of real biogas generated in a methane fermentation reactor to SOFC by using Ni-ScSZ cermet as an anode material. They found that cell voltage above 0.9 V was stably obtained over 50 h at 1273 K (200 mAcm^{-2}) without carbon deposition. They also revealed that the direct-biogas SOFC operated at 1273 K is tolerant to 1 ppm level H_2S contamination.

The direct liquid methanol as the candidate fuel for solid oxide fuel cell was studied by Liu et al. (2008). They chose the traditional fuels such as hydrogen, ammonia, methane and ethanol for comparison. The results demonstrates that when using methanol as a fuel, no coking was detected on anode after running about 160 h but when the cell operated with methane and ethanol as fuels exhibit severe degradation. The researchers explained this from the kinetic factors that molecule structures of these three substances possess quite different characteristics. The C-O bond in methanol easily reacts with oxygen ions from cathode to form CO_2 . In another hand, the H_2O and CO_2 formed from the anode reactions during the cell operation can suppress the carbon formation. Besides, Ni-based anode is a good catalyst to break CH_3OH directly into CO and H_2 , which are the right fuels for SOFC. In CH_4 , however, there is only C-H bonds that coking is possible if C-H bonds break into C and H_2 on the Ni catalysis but no sufficient O^- to react with. While in the case of ethanol molecule, the situation would be surely more severe due to the existence of C-C bonds. Moreover, the cell performances with methanol, humidified H_2 and ammonia as fuels at the same temperatures are also tested and compared. The result showed that the performances of cell fuelled with methanol are lower than hydrogen but higher than ammonia. The differences in performance of the cells are related to the different process of the three fuels involved at anode side, which can be explained by the AC impedance spectroscopy.

3.2 Distillation Process Integrated with the SOFC System.

The thermodynamic assessment of solid oxide fuel cell system fuelled by bioethanol integrated with distillation column was studied by Wassana Jamsak et al. (2007). The SOFC system composed of a distillation column, an EtOH/H₂O heater, an air heater, an anode preheater, a reformer, an SOFC stack and an afterburner. Bioethanol with 5 mol% ethanol was purified in a distillation column to obtain a desired concentration necessary for SOFC operation. The SOFC stack was operated under isothermal conditions. The study showed that it is possible to operate the SOFC–DIS system in an energy self-sufficient mode by adjusting the operating voltage and/or fuel utilization. It was found that higher ethanol concentration yielded higher electrical power (for C_{EtOH} in the range of 15–17%), higher overall electrical efficiency and acceptably high power density. The optimum ethanol recovery is 80%. However, the obtained performance of the SOFC–DIS system was quite low (0.32 Wcm⁻², 173.07 kW, 33.3% overall efficiency based on total ethanol flow rate fed to SOFC–DIS system at $U_f = 80\%$, EtOH recovery = 80% and $C_{\text{EtOH}} = 41\%$). It was found that the reboiler heat duty was the limit of the SOFC–DIS system. Moreover, a huge amount of heat was lost at the condenser.

To improve the performance of the SOFC–DIS system, Wassana Jamsak et al. (2009) investigated The MER (maximum energy recovery) network for SOFC-DIS system. The utilization of internal useful heat sources from within the system and a cathode recirculation has been considered. The utilization of condenser duty for preheating the incoming bioethanol and cathode recirculation for SOFC-DIS system were chosen and implemented to the SOFC-DIS (CondBio-CathRec). Different MER designs were investigated. A heat exchanger loop and utility path were also investigated. It was found that eliminate the high temperature distillate heat exchanger can lower the total cost index. The recommended network is that the hot effluent gas is heat exchanged with the anode heat exchanger, the external reformer, the air heat exchanger, the distillate heat exchanger and the reboiler, respectively. The

corresponding performances of this design are 40.8%, 54.3%, 0.221Wcm^{-2} for overall electrical efficiency, Combine Heat and Power (CHP) efficiency and power density, respectively.

3.3 Membrane for Ethanol/Water Separation in Pervaporation

One of the most important tasks for pervaporation is to develop membranes with high flux and high selectivity. Therefore, there are a lot of research studied and improved the effective membrane for pervaporation. Gu et al. (2009) developed the membrane from silicalite-filled polyether-block-amide (PEBA) membranes for separation of ethanol/water mixtures. In this study, silicalite was added in order to improve the selectivity towards ethanol by improving the hydrophobicity of the membrane. It was found that when a silicalite content is 2.0 wt %, both permeation flux and separation factor reached a maximum value, $833\text{ g/m}^2\text{h}$ and 3.6, respectively. Moreover when the feed concentration and temperature increase, both separation factor and total flux also increased. This result shows the opposite trend with the literature study that selectivity decreases with increasing feed temperature. It can be explained by the fact that the activation energy of ethanol was a little higher than that of water which implies that the organic permeation flux is more sensitive to the increase of temperature compared to that of water permeation flux, so the permeation of ethanol increase faster than that of water then the separation factor increase.

The multiple-layer composites membranes with an alternating silicone/PVDF/silicone configuration were prepared by Chang and Chang (2004). This membrane was tested over the entire composition range of ethanol/water mixtures in pervaporation processes. The separation factor of the composite membrane increased with increasing the thickness of the active silicone layer whereas the permeation flux follows a reversed order. The results indicated that this membrane gave the best performance with a separation factor of 31, permeation rate of $0.9\text{ kg/m}^2\text{ h}$ and PSI of 27,900 at a 10 wt.%

ethanol feed concentration. This membrane demonstrated superb pervaporation performance comparing with traditional membranes that had only one active permselective layer.

Fadeev et al. (2003) investigated the pervaporation recovery of ethanol from yeast fermentation broth using poly[1-(trimethylsilyl)-1-propyne] (PTMSP). They found that the deterioration of PTMSP pervaporation performance in the presence of fermentation broth is caused mainly by factors other than physical or chemical aging or deposition of cells on the PTMSP membrane surface. It was found that free volume of the fouled PTMSP membrane was occupied with the highly sorbing and low volatility by-products of the fermentation broth, most likely with diols. The PTMSP film did not show appreciable deterioration of membrane properties in the pervaporation of aqueous solution of organic compounds with high volatility. The ethanol separation factor is 19.9 and the permeation flux is about $300 \text{ g/m}^2 \text{ h}$.

Lin et al. (2003) studied the preparation of silicalite membrane related to membrane separation properties focusing on in situ crystallization to prepare highly selective silicalite membranes on porous tubular supports by a single hydrothermal treatment. The membrane separation properties were controlled by synthesis conditions such as seeding, temperatures, supports, and silica sources. The results show that the better silicalite membranes, specifically, higher separation selectivities, were prepared by in situ crystallization using the colloidal silica. The highest ethanol/water separation factor was 106 with a flux of $0.9 \text{ kg/m}^2 \text{ h}$ for a feed concentration of 5 wt% ethanol at 333 K.

High-performance silicalite-1 membranes were synthesized via two-step *in-situ* hydrothermal synthesis on novel porous silica tubes by Chen et al. (2007). Improving the separation performance of silicalite-1 membranes was achieved by filling supports with mixed solution and aging before crystallization. After repeated calcinations, silicalite-1 membrane synthesized on silica support showed thermal stability, which suggested that silica supports were more suitable to prepare high-performance silicalite-1 membranes.

Permeation flux and separation factor towards ethanol/water mixture at 333 K were 0.56 kg/m²·h and 84, respectively.

3.4 SOFC modeling.

In order to simplify the study, there are a lot of research used the programs to simulate and set up the experimentation. Ni et al. (2008) developed an electrochemical model to study the methane (CH₄) fed solid oxide fuel cell (SOFC) using proton conducting electrolyte (SOFC-H) and oxygen ion conducting electrolyte (SOFC-O). The result reveals that the actual performance of the CH₄ fed SOFC-H is considerably lower than the SOFC-O, partly due to higher ohmic overpotential of SOFC-H which difference from the previous thermodynamic analyses. The anode concentration overpotentials of the CH₄ fed SOFC-H and SOFC-O are found to decrease with increasing temperature, which is different from previous analyses on the H₂ fed SOFC. The difference between this study and the previous study is due to the fact that H₂ is produced in the CH₄ fed SOFC via methane steam reforming (MSR) and water gas shift (WGS) reactions increase with increasing temperature, more H₂ can be produced at elevated temperatures, and as a result, leading to higher H₂ molar fraction and lower concentration overpotentials. They also found that the microstructure of the SOFC needs to be carefully optimized to attain the minimize electrode total overpotentials.

Arteaga et al. (2008) simulated and evaluated the bioethanol processing system to feed a 200 kW solid oxide fuel cell. The general scheme of the process is composed of vaporization, heating, bioethanol steam reforming (ESR) and SOFC stages. The performance pseudo-homogeneous model of the reactor, consisting of the catalytic ESR using a Ni/Al₂O₃ catalyst, has been developed based on the principles of classical kinetics and thermodynamics through a complex reaction scheme and a Lagmuir-Hishelwood kinetic pattern. The resulting model is employed to evaluate the effect of several design and operation parameters on the process such as tube diameter,

catalyst pellets diameter, temperature, space time and water/ethanol molar ratio. It can be concluded that higher water/ethanol ratio ($R_{AE} = 5:1$) and temperatures (above 773 K) favors hydrogen yield ($Y_H = 4.1$) and selectivity ($S_H = 91\%$). At temperatures above 773K and $R_{AE} > 6$, the reforming efficiencies exhibit a plateau because of the thermodynamics constraints of the process.

Arteaga-Perez et al. (2009) also studied the simulation and heat integration of a solid oxide fuel cell by using Pinch technology to design the heat exchanger network of an ethanol fueled SOFC system. The system and fuel cell efficiencies are studied under different process conditions, temperature, water to ethanol molar ratio and fuel utilization coefficient. The SOFC off gases are mixed and fed to an afterburner providing heat to the process. Two heat exchanger networks were designed being demonstrated that when the fuel utilization coefficient in the SOFC is 80%, the reforming reactor temperature is 823 K and the ethanol to water molar ratio is 1:5.5 then the auto-sustainability condition is reached.

Piroonlerkgul et al., (2008) investigated the suitable reforming reagents for biogas fed SOFC systems which are programmed in Visual Basic. The system configuration divided into three main systems namely, SOFC using steam as the reforming agent (steam-fed SOFC), SOFC using air as the reforming agent (air-fed SOFC) and SOFC using both air and steam as the reforming agents (co-fed SOFC). It was found that steam is considered to be the most suitable reforming agent as the steam-fed SOFC (H_2O : biogas = 1.2, CH_4 : CO_2 in biogas = 60:40 and fuel processing temperature = 873 K) offers much higher power density than the air-fed SOFC (air: biogas = 1.6, CH_4 : CO_2 in biogas = 60:40 and fuel processing temperature 1073 K) although its electrical efficiency is slightly lower due to the high energy requirement in the steam generation. In the case of the co-fed SOFC (H_2O : biogas = 0.8, air: biogas = 2, CH_4 : CO_2 in biogas = 60:40 and fuel processing temperature 973 K), the power density can be improved but the electrical efficiency becomes lower compared with the case of the air-fed SOFC. The biogas split option was considered in order to improve the

electrical efficiency of the steam-fed SOFC. It was found that a higher electrical efficiency can be achieved (overall electrical efficiency = 59%).



ศูนย์วิจัยทรัพยากร
จุฬาลงกรณ์มหาวิทยาลัย

CHAPTER IV

MODELLING

This chapter presents all of the simulation models and calculation procedures for both two different purification processes and the SOFC system. Aspen™ Plus program was used to simulate the purification process in order to find the optimal operating conditions that require the minimum energy consumption. For the SOFC system, the performance analysis was evaluated by visual basic program.

4.1 Bioethanol Purification Process

4.1.1 Distillation Process

The amount and compositions of bioethanol was based on 1,000 kg of cassava chips which is the raw material in this research (Leng et. al., 2008). Since ethanol is the main composition in the fermentation broth then in order to simplify the calculations, the solution is assumed to contain only ethanol and water.

The schematic diagram of this model is shown in Figure 4.1. The distillation column module that used for the simulation was the Radfrac rigorous equilibrium stage distillation equipped with a partial condenser and a kettle boiler. The minimum heat duty can be obtained by adjusting the number of stages, feed stage, reflux ratio and distillate rate for the designed ethanol recovery and purity. The bottom stream may be partially mixed with the distillate stream to obtained designed concentration of ethanol.

The mixing solution was heated up to the reformer temperature by the heater which operate at the temperature of 1023 K and pressure of 1 atm (Wassana Jamsak et al., 2007) before being fed to the external reformer and the SOFC system. The energy

consumption for distillation process composes of condenser duty, reboiler duty and heater duty. It was assumed that the power consumption was neglected due to the less power use for distillation compare to the pervaporation process.

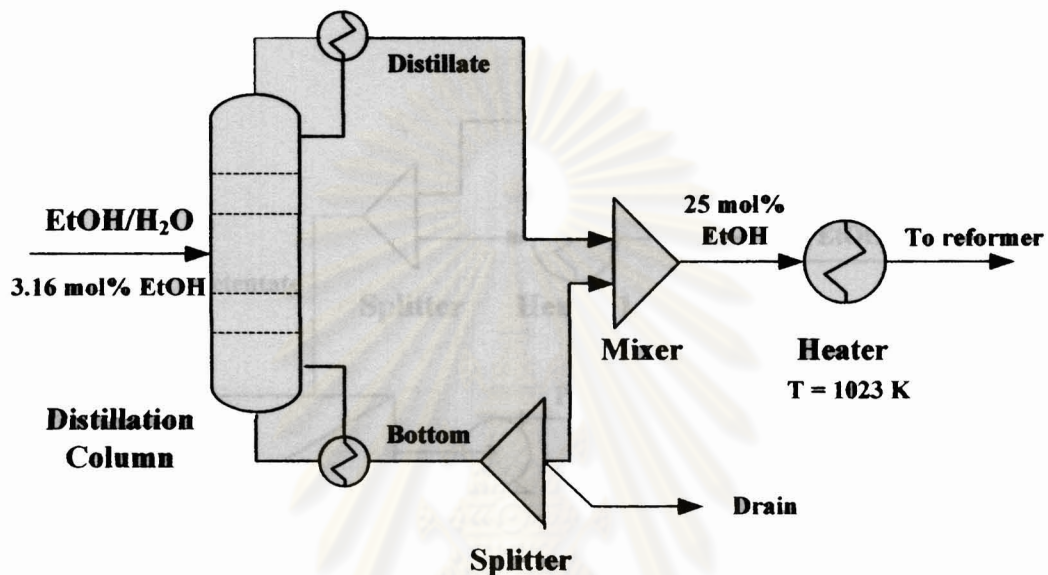


Figure 4.1 The schematic diagram of purification process by distillation

4.1.2 Pervaporation Process

The schematic diagram of the pervaporation process is shown in Figure 4.2. The pervaporation of bioethanol solution was carried out at 333 K (Chen et al., 2008) with two different level of permeate pressure i.e. 0.1 and 0.05 atm. The permeate stream purity depends on the separation factor of the membrane. Therefore, the operating conditions can be obtained by adjusting the separation factor of the membrane. After that the energy and power consumption that required for bioethanol purification to the designed ethanol recovery and purity was calculated. As mentioned earlier, retentate stream may be partially mixed with the permeate stream to obtained 25 mol% ethanol concentration. Since there is the high different level of temperature between two streams

then the retentate stream was preheated to the same temperature as the permeate stream before mixing. After that the mixing stream was heated up to the reformer temperature ($T = 1023$ K) before being fed to the external reformer and the SOFC system.

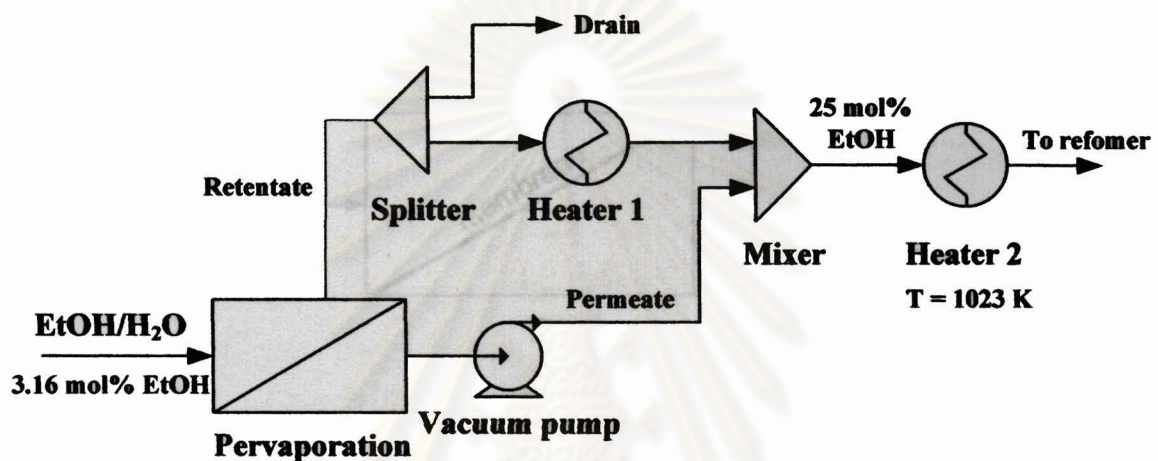


Figure 4.2 The schematic diagram of purification process by pervaporation

The calculation procedure for this process can be divided into two main parts as mass balance and energy balance equations.

4.1.2.1 Mass balance equations

All of the involved variables are expressed in Figure 4.3. The correlation equations are as follow:

$$F = P + R \quad (4.1)$$

$$x_F F = y_P P + x_R R \quad (4.2)$$

$$\text{Recovery} = \frac{y_P P}{x_F F} \quad (4.3)$$

$$\alpha = \frac{y_P / (1 - y_P)}{x_F / (1 - x_F)} \quad (4.4)$$

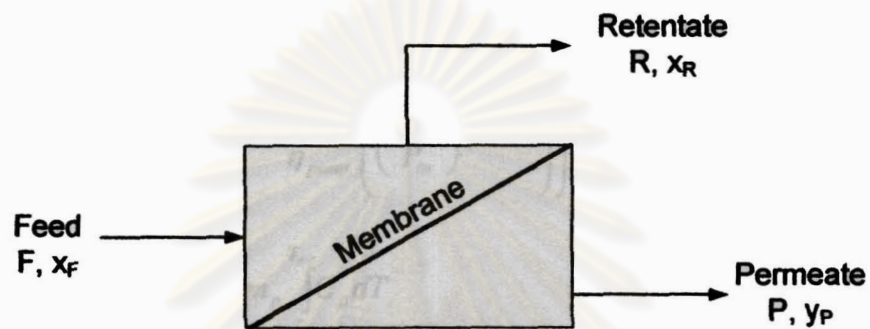


Figure 4.3 The involved variables for mass balance equation

4.1.2.2 Energy balance

From Figure 4.2, the total energy required includes the energy for pervaporation unit, heater 1 heater 2 and the power consumption for vacuum pump. The energy consumption for heater 1 and heater 2 can be obtained from the simulation using Aspen™ Plus program. The energy for pervaporation unit and the power consumption for vacuum pump can be calculated by the following equations.

- Pervaporation unit

$$Q = m \int_{T_n}^{T_{out}} C_p dT + mL \quad (4.5)$$

- Vacuum pump

In this research, the efficiency of the vacuum pump was assumed to be 75%. The outlet gas temperature of vacuum pump and the power consumption can be estimated by using Eqs. (4.6) and (4.7), respectively. (Kaneko et al., 2006)

$$T_{out} = T_{in} \left(1 + \frac{1}{\eta_{pump}} \left(\left(\frac{P_{out}}{P_{in}} \right)^{\frac{\gamma-1}{\gamma}} - 1 \right) \right) \quad (4.6)$$

$$W_{pump} = -m_p \int_{T_{in}}^{T_{out}} C_p dT \quad (4.7)$$

where $\gamma = \frac{C_p}{C_p - R}$ (4.8)

4.2 The SOFC system modelling

This research applied the SOFC modeling from Pakorn Piroonlerkgul et al., (2007) to analyze the performance of SOFC system integrated with two different purification processes. The SOFC system modeling have been verified with the experimental results of Zhao et al., (2005) and Tao et al., (2005) at the high concentration of hydrogen in feed (mole fraction of hydrogen = 0.97) and also verified with the experimental results of Petruzzi et al., (2003) at the low concentration of hydrogen in feed (mole fraction of hydrogen = 0.26). It was found that the simulation results showed good agreement with those from the literatures.

The schematic diagram of SOFC system is shown in Figure 4.4. The system composes of the external reformer, SOFC stack, afterburner, heater and cooler. It should

be noted that although the DIR operation provides the highest effectiveness in term of energy aspect but the route to produce hydrogen in the commercial applications is very complex. Therefore, the ER-SOFC operation is used in the study.

The 25 mol% concentration of ethanol from the purification process was fed to the external reformer which was simulated by AspenTM plus program and the calculation was based on phase and chemical equilibrium. In order to simplify the calculations, the reformer was assumed to operate isothermally and the outlet gas reaches its equilibrium composition. After that the reformed gas which assumed to contain only 6 components i.e. H₂, CO₂, CO, H₂O, CH₄ and C₂H₅OH were fed to the anode chamber while excess air (500%) was preheated and introduced to the cathode chamber of the SOFC stack. The electrochemical reactions as illustrated in Eqs. (4.9) and (4.10) take place in the SOFC stack and the unreacted fuel was burnt in the afterburner which was assumed to obtain the complete combustion. The exhaust gas was cooled and discharged to the environmental at 403 K.

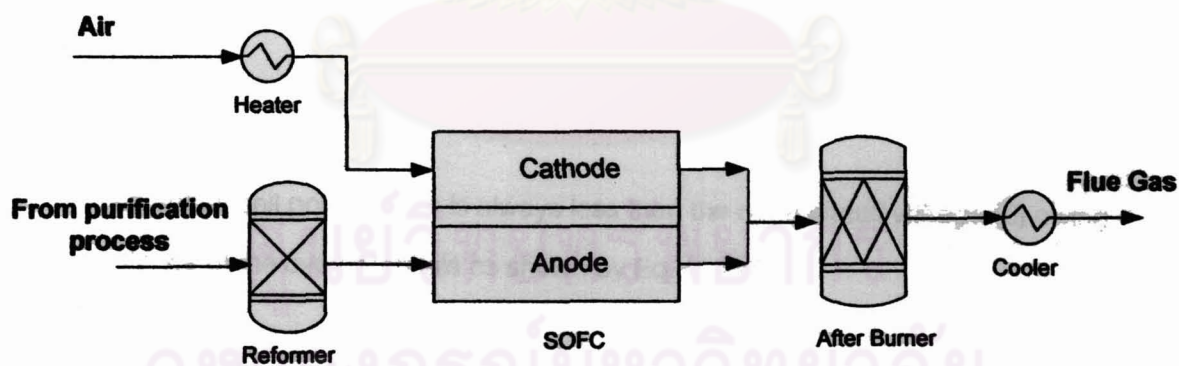
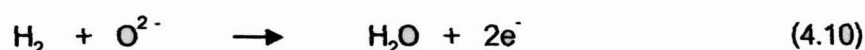
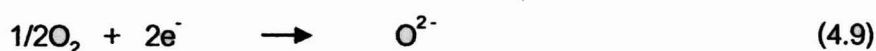


Figure 4.4 The schematic diagram of the SOFC system



For SOFC stack, the Ni-YSZ, YSZ and LSM-YSZ were used as the materials for the anode, electrolyte and cathode respectively. Since the H₂ electro-oxidation is much faster than CO electro-oxidation then it was assumed that only hydrogen ions reacted with oxygen ions and the gas compositions at the anode are always at their equilibrium along the cell length.

The electrochemical model and the calculation procedures are expressed as the following section.

4.2.1 Electrochemical Model

4.2.1.1 Open circuit voltage

The open circuit voltage (E) can be calculated from the Nernst equation as expressed in Eq. (4.11)

$$E = E_0 + \frac{RT}{2F} \ln \left(\frac{P_{H_2} P_{O_2}^{1/2}}{P_{H_2O}} \right) \quad (4.11)$$

The actual cell potential (V) is always less than the open circuit voltage (E) owing to the existence of the overpotentials as shown by Eq. (4.12)

$$V = E - \eta_{act} - \eta_{ohmic} - \eta_{conc} \quad (4.12)$$

4.2.1.2 Overpotentials

The overpotentials are divided into three types: ohmic overpotential (η_{ohmic}), activation overpotential (η_{act}) and concentration overpotential (η_{conc}) which can be explained as below:

- Ohmic overpotential

The ohmic overpotential is the resistance of the electron to flow through the electrodes, interconnections and electrolyte. This overpotential is the major loss of the SOFC stack which can be calculated from Eq. (4.13)

$$\eta_{ohmic} = 2.99 \times 10^{-11} iL \exp\left(\frac{10300}{T}\right) \quad (4.13)$$

- Activation overpotential

The activation overpotential occurs from the electrochemical reaction at the electrodes. Normally, the activation overpotential dominates at low current density but at high temperature, the reaction rate is very fast then this value is small. This overpotential can be expressed by the Butler-Volmer equation.

$$i = i_0 \left[\exp\left(\frac{\alpha z F \eta_{act}}{RT}\right) - \exp\left(-\frac{(1-\alpha) z F \eta_{act}}{RT}\right) \right] \quad (4.14)$$

In case of SOFC, the value of α and z are 0.5 and 2 respectively. Consequently, the activation overpotential at anode and cathode side can be written as:

$$\eta_{act} = \frac{RT}{F} \sinh^{-1} \left(\frac{i}{2i_0} \right) \quad (4.15)$$

The exchange current density (i_0) for the cathode and anode side can be calculated from these two equations:

$$i_{o,a} = \gamma_a \left(\frac{P_{H_2}}{P_{ref}} \right) \left(\frac{P_{H_2O}}{P_{ref}} \right) \exp \left(-\frac{E_{act,a}}{RT} \right) \quad (4.16)$$

$$i_{o,c} = \gamma_c \left(\frac{P_{O_2}}{P_{ref}} \right)^{0.25} \exp \left(-\frac{E_{act,c}}{RT} \right) \quad (4.17)$$

- Concentration overpotential

The concentration overpotential is the loss due to the different concentration of gas between the bulk and the reaction site. It can be estimated by eqs. (4.18) and (4.19)

$$\eta_{conc,a} = \frac{RT}{2F} \ln \left[\frac{\left(1 + \left(\frac{RT}{2F} \right) \left(\frac{l_a}{D_{a(eff)} P_{H_2O}^l} \right) i \right)}{\left(1 - \left(\frac{RT}{2F} \right) \left(\frac{l_a}{D_{a(eff)} P_{H_2}^l} \right) i \right)} \right] \quad (4.18)$$

$$\eta_{conc,c} = \frac{RT}{4F} \ln \left[\frac{p_{O_2}^I}{(P_c - \delta_{O_2}) - ((P_c - \delta_{O_2}) - p_{O_2}^I) \exp \left[\left(\frac{RT}{4F} \right) \left(\frac{\delta_{O_2} l_c}{D_{c(eff)} P_c} \right) i \right]} \right] \quad (4.19)$$

δ_{O_2} , $D_{a(eff)}$ and $D_{c(eff)}$ can be expressed by:

$$\delta_{O_2} = \frac{D_{O_2,k(eff)}}{D_{O_2,k(eff)} + D_{O_2-N_2(eff)}} \quad (4.20)$$

$$D_{a(eff)} = \left(\frac{P_{H_2O}}{P_a} \right) D_{H_2(eff)} + \left(\frac{P_{H_2}}{P_a} \right) D_{H_2O(eff)} \quad (4.21)$$

$$\frac{1}{D_{c(eff)}} = \frac{\xi}{n} \left(\frac{1}{D_{O_2,k}} + \frac{1}{D_{O_2-N_2}} \right) \quad (4.22)$$

$$\frac{1}{D_{H_2(eff)}} = \frac{\xi}{n} \left(\frac{1}{D_{H_2,k}} + \frac{1}{D_{H_2-H_2O}} \right) \quad (4.23)$$

$$\frac{1}{D_{H_2O(eff)}} = \frac{\xi}{n} \left(\frac{1}{D_{H_2O,k}} + \frac{1}{D_{H_2-H_2O}} \right) \quad (4.24)$$

Eq. (4.25) shows the relation between effective parameter ($D_{(eff)}$) and nominal parameter (D):

$$D_{(eff)} = \frac{n}{\xi} D \quad (4.25)$$

The correlation below is used to calculate the Knudsen diffusivity:

$$D_{i,K} = 9700 \sqrt{\frac{T}{M_A}} \quad (4.26)$$

The Chapman-Enskog equation is used for calculating the ordinary diffusivity:

$$D_{A-B} = 1.8583 \times 10^{-3} \left(\frac{T^{3/2} \left(\left(\frac{1}{M_A} \right) + \left(\frac{1}{M_B} \right) \right)^{1/2}}{P \sigma_{AB}^2 \Omega_D} \right) \quad (4.27)$$

where σ_{AB} and Ω_D can be calculated from the following equations.

$$\sigma_{AB} = \frac{\sigma_A + \sigma_B}{2} \quad (4.28)$$

$$\Omega_D = \frac{A}{T_k^B} + \frac{C}{\exp(D \cdot T_k)} + \frac{E}{\exp(F \cdot T_k)} + \frac{G}{\exp(H \cdot T_k)} \quad (4.29)$$

where T_k is equal to T / ϵ_{AB} and A, C, E and G are constants for each gas.

The overall efficiency of the system can be computed by Eq. (4.30):

$$\% \text{Overall electrical efficiency} = \frac{W_{e,net}}{n_{EtOH} LHV_{EtOH}} \times 100\% \quad (4.30)$$

The overall parameters used in this model are summarized in Table 4.1.

Table 4.1 Summary of model parameters

Parameters	Value	Parameters	Value
l_e (μm)	50	σ_{H_2} (\AA)	2.827
$E_{act,a}$ (J/mol)	1.0×10^5	σ_{H_2O} (\AA)	2.641
$E_{act,c}$ (J/mol)	1.2×10^5	σ_{N_2} (\AA)	3.798
γ_a (A/m^2)	1.344×10^{10}	σ_{O_2} (\AA)	3.467
γ_c (A/m^2)	2.051×10^9	ε_{H_2}	59.7
l_a (μm)	750	ε_{H_2O}	809.1
l_c (μm)	50	ε_{N_2}	71.4
ξ (μm)	5.4	ε_{O_2}	106.7
n	0.48		

4.2.2 Calculation Procedures

In order to calculate the current and the area of the SOFC stack, the SOFC stack was separated into the small region which has equal fuel utilization as shown in Figure 4.5.

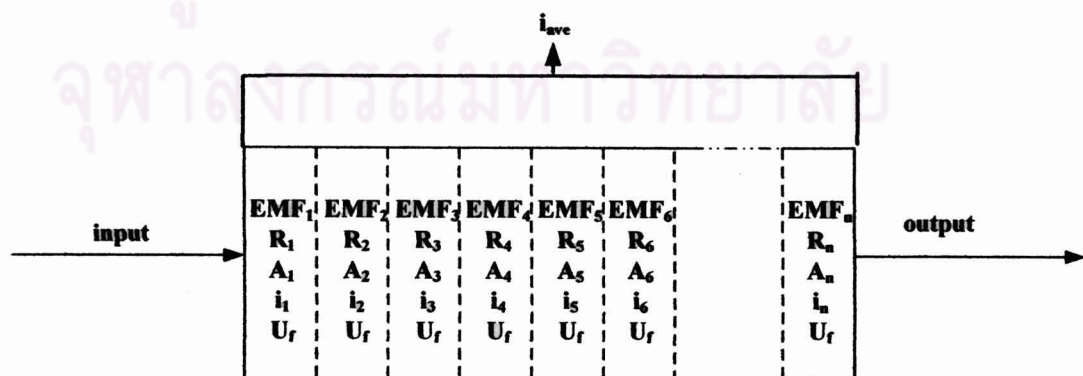


Figure 4.5 The SOFC stack area separation for the calculation

The calculation procedures are as follow

4.2.2.1 Define the final fuel utilization and operating voltage. The fuel utilization step size is 0.01.

4.2.2.2 The electrochemical calculation performs using the sets of equations shown in section 4.2.1. Open circuit voltage (E) is initially computed. Afterward, the current density is estimated until the difference between E and the total overpotentials is equal to the operating voltage (V).

4.2.2.3 The SOFC area of this fuel utilization region is calculate from the following equation

$$A_f = \frac{2F(\Delta U_f)}{i_f} \quad (4.31)$$

The calculations are recomputed until the value of U_f reached the final fuel utilization. Then the current density (i_{ave}), the power density (p_{ave}) and the total electricity (W_e) are calculated employing Eqs. (4.32), (4.33) and (4.34), respectively.

$$i_{ave} = \frac{2F(U_{f,final})}{A_{total}} \quad (4.32)$$

$$p_{ave} = i_{ave}V \quad (4.33)$$

$$W_e = \frac{p_{ave}}{A_{total}} \quad (4.34)$$

The flow chart of the program calculation procedure is shown in Figure 4.6

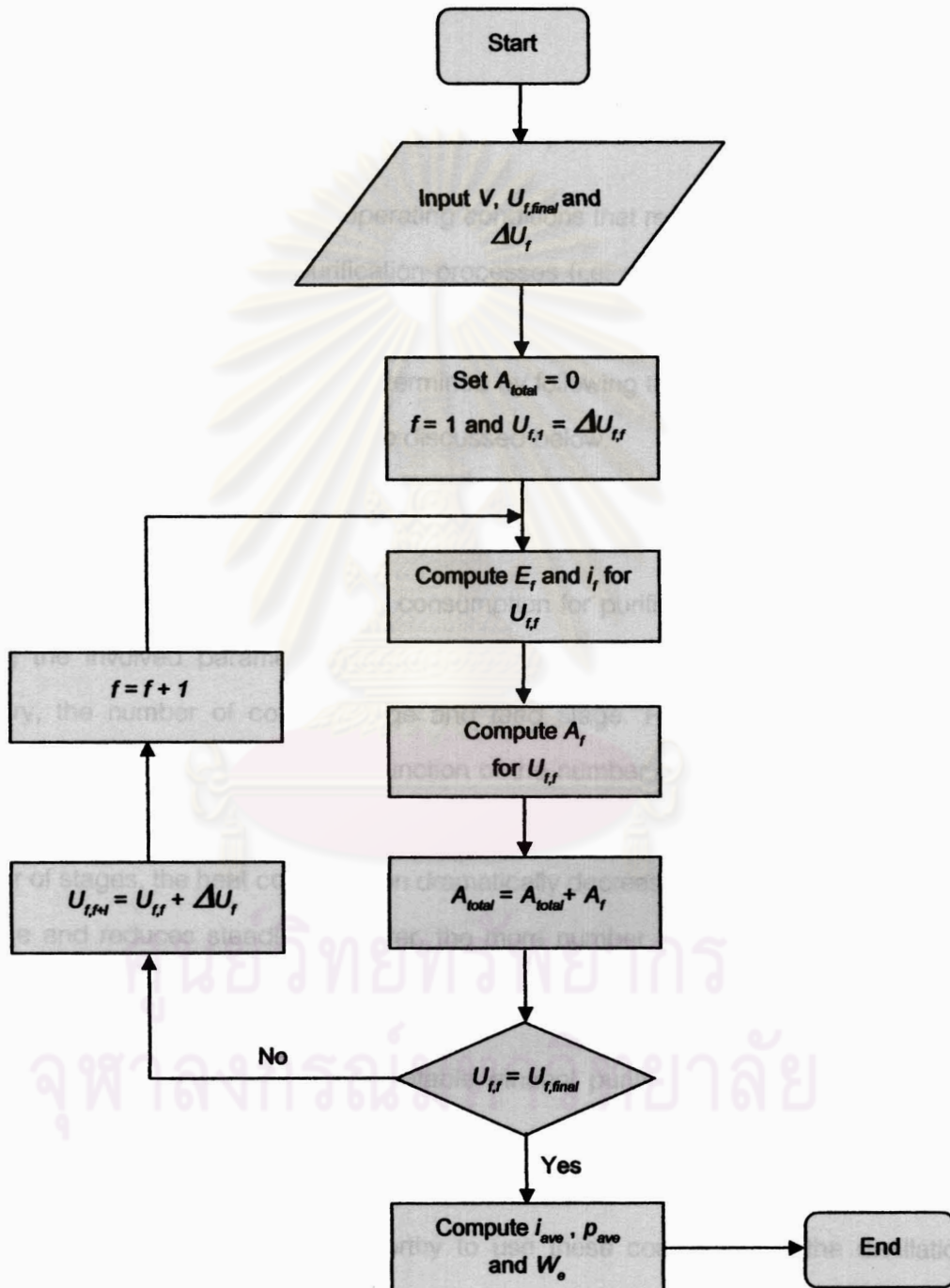


Figure 4.6 The flow chart of the program calculation procedures

CHAPTER V

RESULTS AND DISCUSSION

5.1 The optimal operating conditions for bioethanol purification

In this section, the optimal operating conditions that require the minimum energy consumption for two different purification processes (i.e. distillation and pervaporation) were investigated. The total heat and electrical power consumption for both distillation and pervaporation processes were determined by following the details described earlier in the modeling section. The results are discussed below.

5.1.1 Distillation

As mentioned before, the heat consumption for purification can be obtained by varying the involved parameters, i.e. ethanol purity in the distillate stream, ethanol recovery, the number of column stage and feed stage. Figure 5.1 shows the heat consumption for distillation unit as a function of the number of column stage. It can be seen that less heat required when operates at more number of stages. When increasing number of stages, the heat consumption dramatically decreases initially at lower number of stage and reduces steadily; however, the more number of stages mean that more capital cost for distillation column is needed.

It was found that there is a suitable ethanol purity for the purification which requires the minimum total heat consumption. For example, from Figure 5.2 with ethanol recovery of 90%, the purification to 35 mol% concentration of ethanol requires less total heat consumption. Therefore, it is worthy to use these conditions for the distillation column. The optimal operating conditions for different ethanol recoveries are summarized in Table 5.1. The results show that when the distillation column operates in order to achieve the higher ethanol recovery, more heat is required.

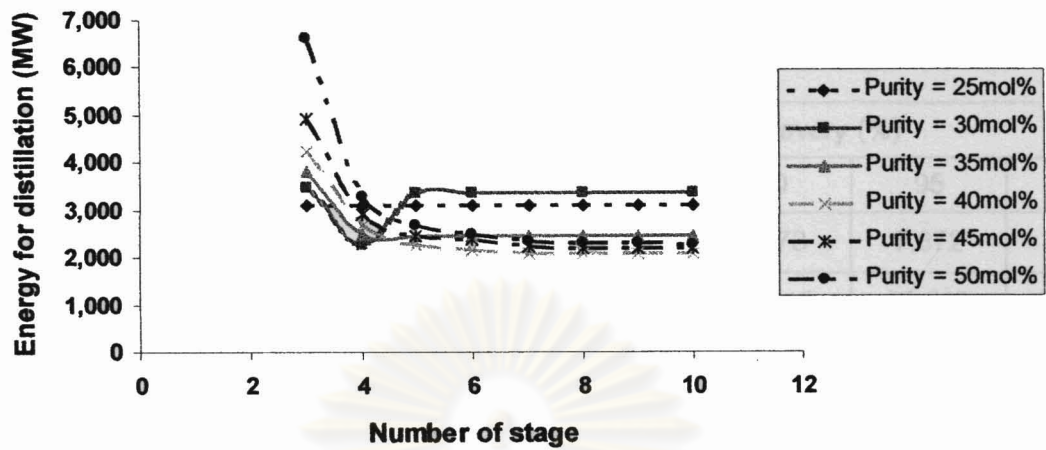


Figure 5.1 Effect of ethanol purity on the heat consumption (Q) for distillation column (Ethanol recovery = 90%)

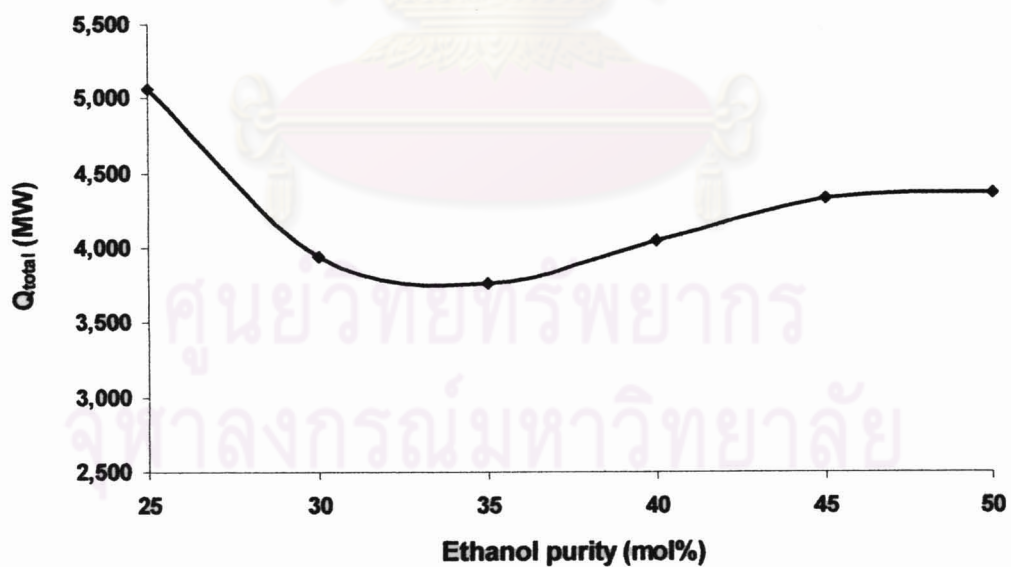


Figure 5.2 Effect of the ethanol purity on the total heat consumption (Q_{net}) for distillation column (Ethanol recovery = 90%)

Table 5.1 The total heat consumption and the optimal operating conditions for bioethanol purification by distillation process

Conditions	Ethanol recovery (%)				
	80	85	90	95	99
Ethanol flow rate (mol/s)	6,685	7,059	7,473	7,872	8,191
Water flow rate (mol/s)	20,055	21,164	22,419	23,617	24,625
Total flow rate (mol/s)	26,740	28,222	29,891	31,489	32,816
Ethanol purity (mol %)	40	30	35	35	35
Number of stage	5	4	5	6	7
Feed stage	2	2	2	2	2
Total heat consumption (MW)	3,580	3,537	3,763	3,818	4,104

5.1.2 Pervaporation

For pervaporation, the vacuum pump was installed in order to reduce the operating pressure at the membrane permeate side. Two different pressures at the permeate side were investigated, i.e. 0.1 and 0.05 atm. The total heat and electrical power consumption can be calculated by varying the separation factor and the ethanol recovery. The effect of separation factor on the ethanol purity at permeate stream and the permeate flow rate is shown in Figure 5.3. It was found that there is the minimum separation factor for bioethanol purification to achieve a desired ethanol concentration (25 mol%). From Figure 5.3, when the separation factor increases, the ethanol purity at permeate stream also increases while the permeate flow rate decreases. The permeate flow rate reduces dramatically at the beginning and steadily reduces after the separation factor of about 200. For the effect of ethanol recovery, the permeate flow rate increases with increasing the ethanol recovery since more ethanol is recovered at high recovery than that at low recovery.

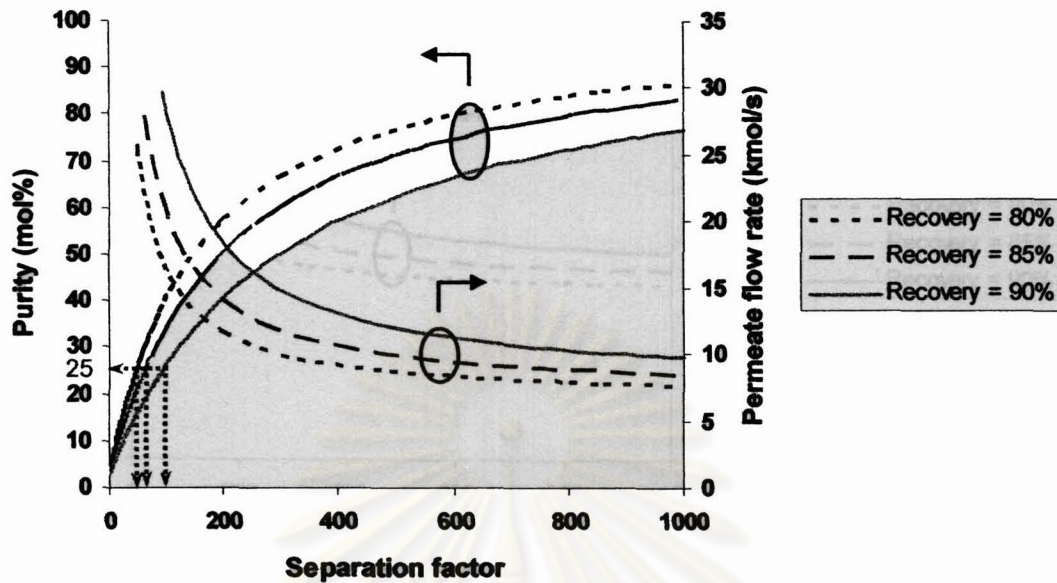


Figure 5.3 Effect of the separation factor on the ethanol purity at permeate stream and the permeate flow rate

Figure 5.4 shows the effect of the separation factor on the total heat (Q_{total}) and electrical power consumption ($W_{e, total}$). It can be seen that when the separation factor increases, the heat consumption increases significantly particularly at low separation factors and then gradually increases at higher separation factors. The opposite trend was observed for the electrical power consumption. This is because the electrical power consumption depends on the flow rate of the permeate which continuously decreases at higher separation factors due to the higher ethanol purity achieved, and therefore, higher amount of heat is demanded to preheat water in the retentate for mixing with purified ethanol to obtain the reformer feed at a desired ethanol concentration (25 mol%). It should be noted that in order to compare the energy requirements for the operations at different values of ethanol recovery and permeate pressure, the membrane separation factor was kept at the value that provide the permeate ethanol purity near 25 mol%.

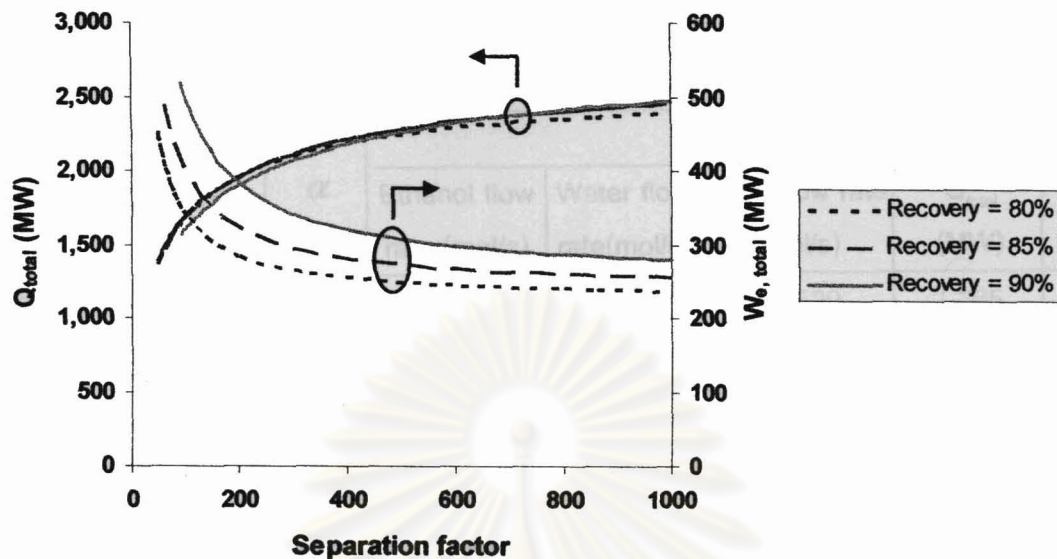


Figure 5.4 Effect of the separation factor on the total heat (Q_{total}) and electrical power consumption ($W_{e, total}$) (Permeate pressure = 0.1 atm)

The optimal operating conditions for two different pressures at the permeate side are summarized in Table 5.2. It can be seen that the lowering of pressure at the permeate side offers lower heat consumption and higher electrical power consumption. This is because when the system operates at low permeate pressure, the temperature of the permeate stream is higher than that at the high permeate pressure (see Eq. 4.6) and hence the heat consumption for preheating the permeate stream to the reformer temperature decreases. In case of the electrical power, the lowering of pressure at the permeate side offers higher electrical power consumption since it requires more electrical power for vacuum pump operation.

Table 5.2 The total heat and electrical power consumption and the optimal operating conditions for bioethanol purification by pervaporation process (25 mol% of ethanol)

Permeate pressure (atm)	Ethanol Recovery (%)	α	Conditions				
			Ethanol flow rate (mol/s)	Water flow rate (mol/s)	Total flow rate (mol/s)	Q_{total} (MW)	$W_{e,total}$ (MW)
0.10	80	49	6,630	19,890	26,520	1,365	453
	85	63	7,041	21,123	28,164	1,459	489
	90	94	7,455	22,365	29,820	1,566	518
	95	186	7,866	23,597	31,463	1,670	548
	99	923	8,199	24,596	32,794	1,755	572
0.05	80	49	6,630	19,890	26,520	1,143	680
	85	63	7,041	21,123	28,164	1,219	733
	90	94	7,455	22,365	29,820	1,312	776
	95	186	7,866	23,597	31,463	1,402	821
	99	923	8,199	24,596	32,794	1,475	856

5.1.3 Comparison between distillation and pervaporation

Table 5.3 shows the total heat and electrical power consumption between distillation and pervaporation processes. It was found that pervaporation process requires less heat consumption than distillation process but it requires the additional electrical power for vacuum pump operation. Moreover, the lowering of pressure at the permeate side requires the higher electrical power consumption because it requires more electrical power to generate less pressure.

Table 5.3 The total heat and electrical power consumption comparison between distillation and pervaporation process

Ethanol recovery (%)	Total heat consumption (MW)			Total power consumption (MW)		
	Distillation	Pervaporation		Distillation	Pervaporation	
		0.1 atm	0.05 atm		0.1 atm	0.05 atm
80	3,580	1,365	1,143	0	453	680
85	3537	1,459	1,219	0	489	733
90	3,763	1,566	1,312	0	518	776
95	3818	1,670	1,402	0	548	821
99	4,104	1,755	1,475	0	572	856

5.2 Performance of SOFC system at the base condition

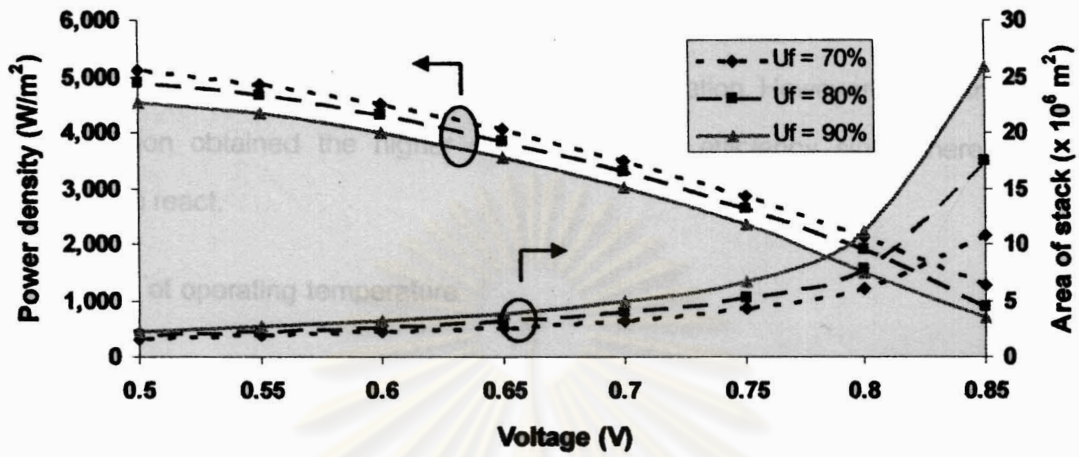
In this section, the effect of the operating conditions such as voltage, temperature, fuel utilization and ethanol recovery on the performance of the SOFC system, i.e. power density, area of SOFC stack, heat of the SOFC stack (Q_{SOFC}), the net useful heat (Q_{net}) and electrical efficiency at the base condition have been investigated.

5.2.1 Effect of operating voltage

Figure 5.5 represents the effect of operating voltage and fuel utilization on the power density, area of SOFC stack, electrical efficiency and net useful heat (Q_{net}) which is the difference between the exothermic heat (SOFC stack and afterburner) and the endothermic heat (heaters and reformer) of the SOFC system.

From Figure 5.5(a), it can be seen that at all values of fuel utilization, the power density decreases when operating at the higher operating voltage while the area of stack increases. Therefore, the operating voltage should not be too high because it requires the larger area of SOFC stack and more cost consumed.

(a)



(b)

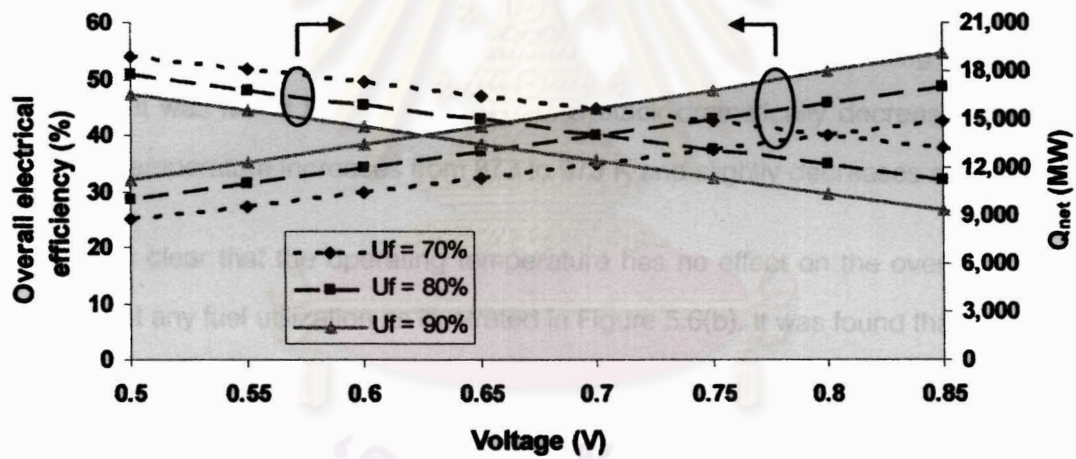


Fig. 5.5 Effect of operating voltage and fuel utilization on (a) the power density and the area of SOFC stack and (b) the electrical efficiency and the net useful heat (Q_{net}) (Ethanol recovery = 80%, Temperature = 1073 K)

At low operating voltage, there is the higher heat generation from the SOFC stack. This leads to the lower overall electrical efficiency as shown in Figure 5.5(b). In

addition, operating at low fuel utilization remains more unreacted fuel exiting the SOFC stack which is burnt in the afterburner and produce more combustion energy to compensate heat loss. Then net useful heat (Q_{net}) in the SOFC system at low fuel utilization operating is higher than that at high fuel utilization. However, operating at high fuel utilization obtained the higher overall electrical efficiency since there is more hydrogen to react.

5.2.2 Effect of operating temperature

The effect of operating temperature is shown in Figure 5.6. Since the higher power density can be obtained when decreasing total resistance and it was found that total resistance decreases when operating at high temperature. This leads to obtain the higher power density at high operating temperature which is shown in Figure 5.6(a). On the other hand, the area of SOFC stack decreases when the operating temperature increases. It was found that the area of SOFC stack dramatically decreases when the operating temperature increases from 873 to 973 K and slightly decreases after 973 K.

It is clear that the operating temperature has no effect on the overall electrical efficiency at any fuel utilization as illustrated in Figure 5.6(b). It was found that although it requires more heat energy for increasing the fuel temperature but after the hot gas left from the SOFC stack and was burnt and cooled down, the heat energy was recovered. Therefore, the temperature has no effect on the power and heat energy hence the overall electrical efficiency of the SOFC system is constant. As mentioned earlier, higher fuel utilization provides more hydrogen to react then the overall electrical efficiency is higher than that at low fuel utilization. It can be seen that heat of the SOFC stack (Q_{SOFC}) decreases as operating temperature increases. However, operating at high temperature may damage the physical property of the SOFC component though it requires less area of SOFC stack as seen in Figure 5.6(a). Therefore, it should be better not to operate the system at too high operating temperature. From the results, it is worthy to note that the development of the cell components is very important task.

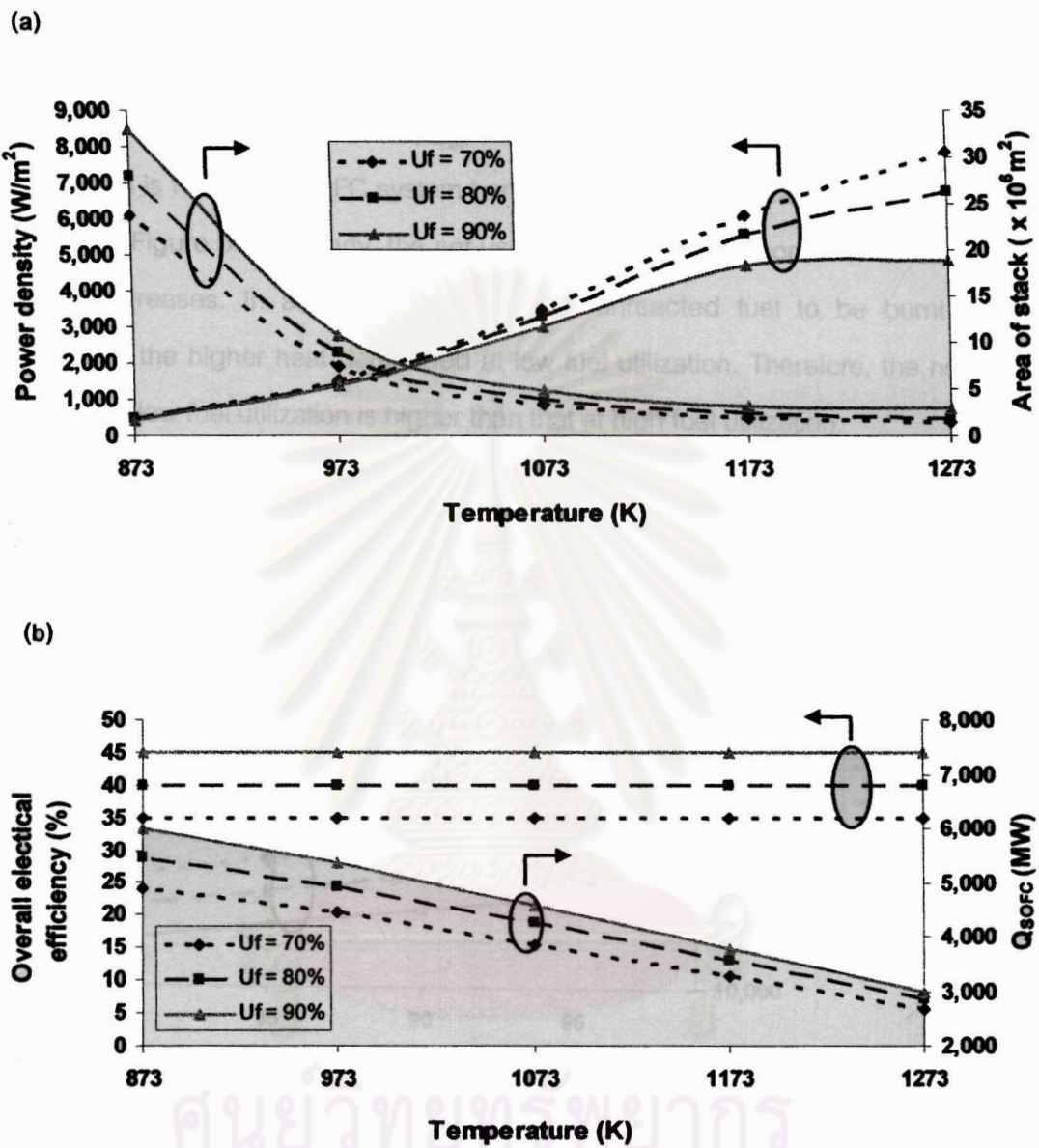


Figure 5.6 Effect of the operating temperature and fuel utilization on (a) the power density and the area of SOFC stack and (b) the overall electrical efficiency and heat of the SOFC stack (Q_{SOFC}) (Ethanol recovery = 80%, Voltage = 0.7 V)

5.2.3 Effect of ethanol recovery

Figure 5.7 presents the effect of ethanol recovery on the overall electrical efficiency and the net useful heat (Q_{net}). At high ethanol recovery and fuel utilization, more ethanol is fed to the SOFC system hence the overall electrical efficiency increases as shown in Figure 5.7. Similarly, the net useful heat (Q_{net}) also increases as the ethanol recovery increases. In addition, there is more unreacted fuel to be burnt and to compensate the higher heat demanded at low fuel utilization. Therefore, the net useful heat (Q_{net}) at low fuel utilization is higher than that at high fuel utilization.

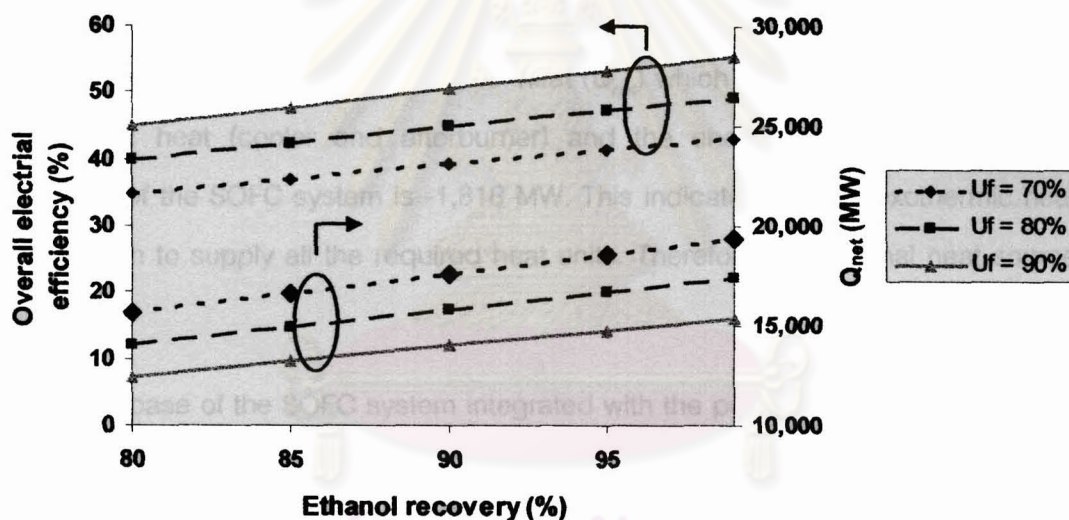


Fig. 5.7 Effect of the ethanol recovery and fuel utilization on the overall electrical efficiency and the net useful heat (Q_{net}) (Voltage = 0.7 V, Temperature = 1073 K)

5.3 Performance of SOFC integrated with two different purification processes

This section investigates and compares the performances of the SOFC systems integrated with the different purification units (i.e., a distillation column and pervaporation). The results are discussed below.

5.3.1 Performances at the base conditions

The operating temperature and the energy requirement for all important units in the SOFC system integrated with the distillation process and pervaporation process at the base conditions are shown in Figure 5.8 and Figure 5.9 respectively. For the SOFC system integrated with the distillation process (Ethanol recovery = 80%, Voltage = 0.7 V, $C_{\text{EtOH, distillate}} = 40$ mol% and Fuel utilization = 70%), the system achieved the electrical power (W_e) of 3,792 MW. The net useful heat (Q_{net}) which is the difference between the exothermic heat (cooler and afterburner) and the endothermic heat (heaters and reformer) of the SOFC system is -1,818 MW. This indicates that the exothermic heat is not enough to supply all the required heat units. Therefore, an external heat source is required.

In case of the SOFC system integrated with the pervaporation process (Ethanol recovery = 80%, Voltage = 0.7 V, $C_{\text{EtOH, permeate}} = 25.7$ mol%, Separation factor of the membrane = 49, Fuel utilization = 70%, Permeate pressure = 0.1 atm), the electrical power (W_e) of 3,761 MW is achieved. Moreover, the system requires the additional electrical power for vacuum pump operation hence the net electrical power ($W_{e,\text{net}}$) of the system is 3,308 MW. It can be seen that the electrical power (W_e) is slightly lower than that in the SOFC system integrated with the distillation process. However, when considering the net useful heat (Q_{net}), it was found that the net useful heat (Q_{net}) of this system is 383 MW. This results show that there is some extra heat left from the system and the system can operate without requiring the external heat source.

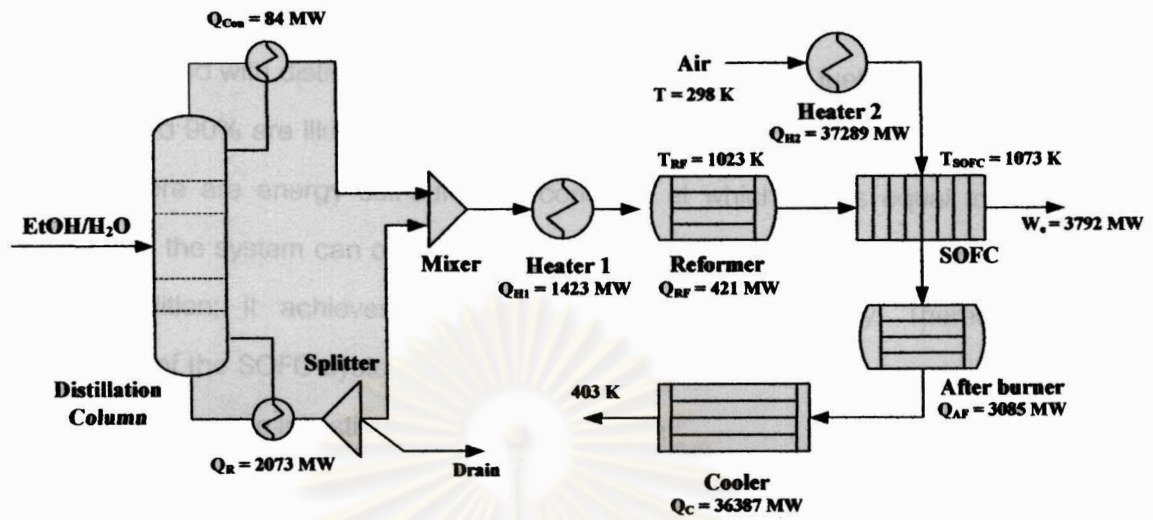


Figure 5.8 Energy and temperature for various units in SOFC system integrated with distillation process (Ethanol recovery = 80%, Voltage = 0.7 V, $C_{EtOH, distilate} = 40$ mol%, Fuel utilization = 70%)

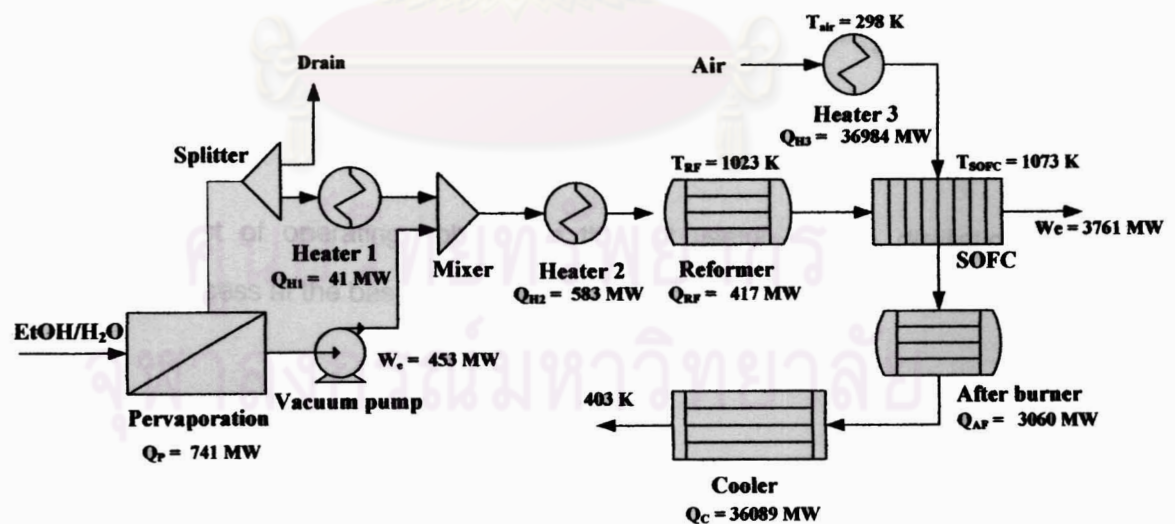


Figure 5.9 Energy and temperature for various units in SOFC system integrated with pervaporation process (Ethanol recovery = 80%, Voltage = 0.7 V, $C_{EtOH, permeate} = 25.7$ mol%, Separation factor = 49, Fuel utilization = 70%, Permeate pressure = 0.1 atm)

The effect of the operating voltage on the net useful heat (Q_{net}) for the SOFC system integrated with distillation and pervaporation processes at fuel utilization equal to 70%, 80% and 90% are illustrated in Figure 5.10, 5.11 and 5.12 respectively. It can be seen that there are energy self-sufficient condition at which Q_{net} is equal to zero. It indicates that the system can operate without the requiring of external heat source and at this condition; it achieves the maximum electrical efficiency. Therefore, the performance of the SOFC system integrated with two different purification processes at Q_{net} equal to zero were investigated in the next section.

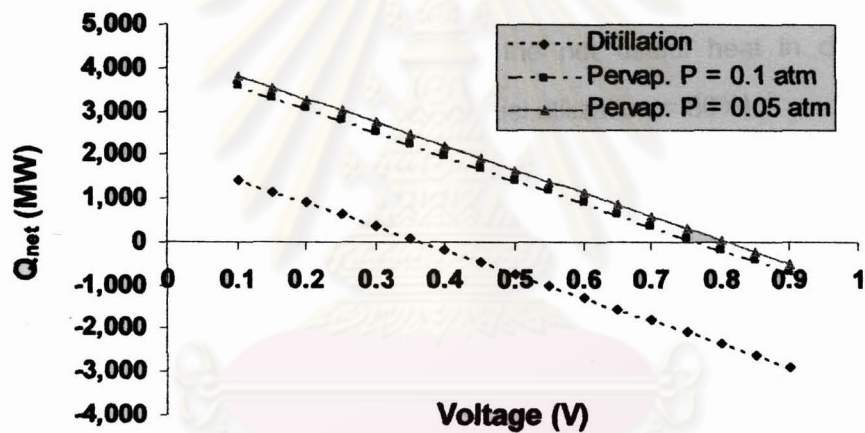


Figure 5.10 Effect of operating voltage on the net useful heat in distillation and pervaporation process at the base condition (Fuel utilization = 70%)

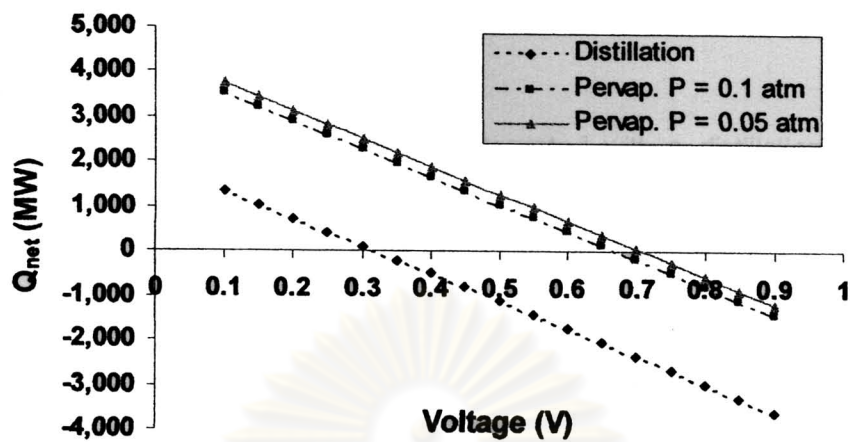


Figure 5.11 Effect of operating voltage on the net useful heat in distillation and pervaporation process at the base condition (Fuel utilization = 80%)

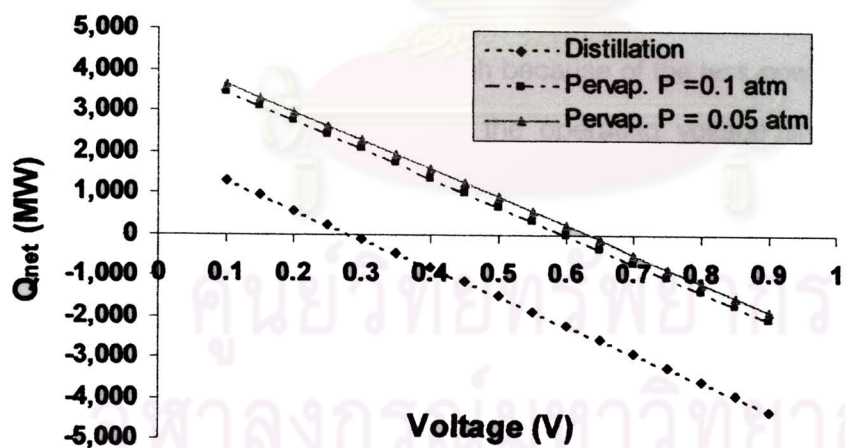


Figure 5.12 Effect of operating voltage on the net useful heat in distillation and pervaporation process at the base condition (Fuel utilization = 90%)

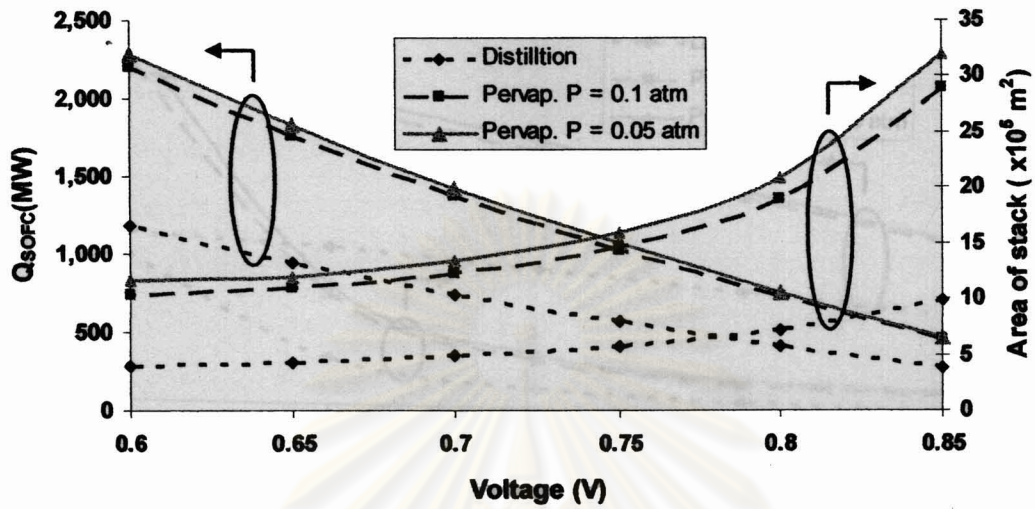
5.3.2 The appropriate operating conditions for SOFC system integrated with the purification process ($Q_{net} = 0$)

The performances of SOFC system integrated with a distillation column and pervaporation processes were investigated and compared. The integrated system was operated at the net useful heat (Q_{net}) equal to zero conditions because, as mentioned earlier, it achieves the maximum electrical efficiency for the overall system without requiring the external heat source. The excessive heat from the SOFC system can supply to the purification units which require the energy. The influence of the operating conditions for the SOFC system such as operating voltage, operating temperature and ethanol recovery on the performances of the SOFC system was investigated.

Figure 5.13 indicates that when the operating voltage is between 0.5 and 0.8 V, the area of SOFC stack starts to increase gradually and dramatically increases at the operating voltage greater than 0.8 V. In contrast, both of the heat of SOFC stack (Q_{SOFC}) and the power density increase with increasing the operating voltage. Although the heat of SOFC stack decreases when the operating voltage increases but the appropriate operating voltage should not be too high because of the less power density obtained at the high operating voltage. Similarly, the operating voltage should not be too low because of more heat generate from SOFC stack (Q_{SOFC}).

The effect of operating temperature is illustrated in Figure 5.14. It was found that the area of SOFC stack dramatically decreases when the operating temperature rises from 873 to 973 K and reduces gradually after 973 K. Moreover, the heat of SOFC stack (Q_{SOFC}) decreases with increasing the operating temperature while the power density increases. Therefore, the operating temperature should not be too low because it may cause the excessive heat generated in the SOFC stack which can directly damage the thermophysical property of the cell components and it also requires more area of SOFC stack. However, too high operating temperature is not recommended because of the limited of the SOFC components' material and the complicated control system for the operation.

(a)



(b)

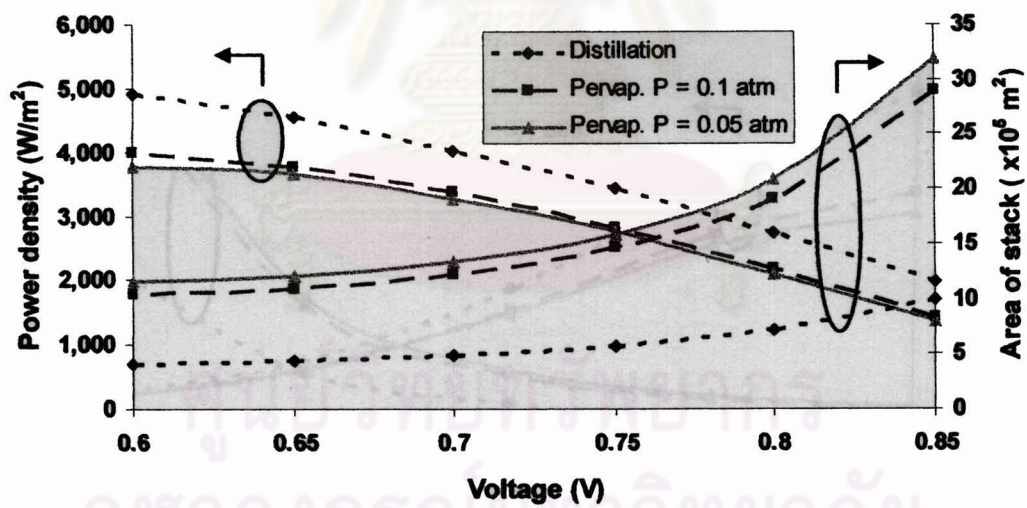


Figure 5.13 Effect of the operating voltage on (a) the heat of SOFC stack (Q_{SOFC}) and the area of SOFC stack and (b) the power density and the area of SOFC stack (Ethanol recovery = 80%, Temperature = 1073 K)

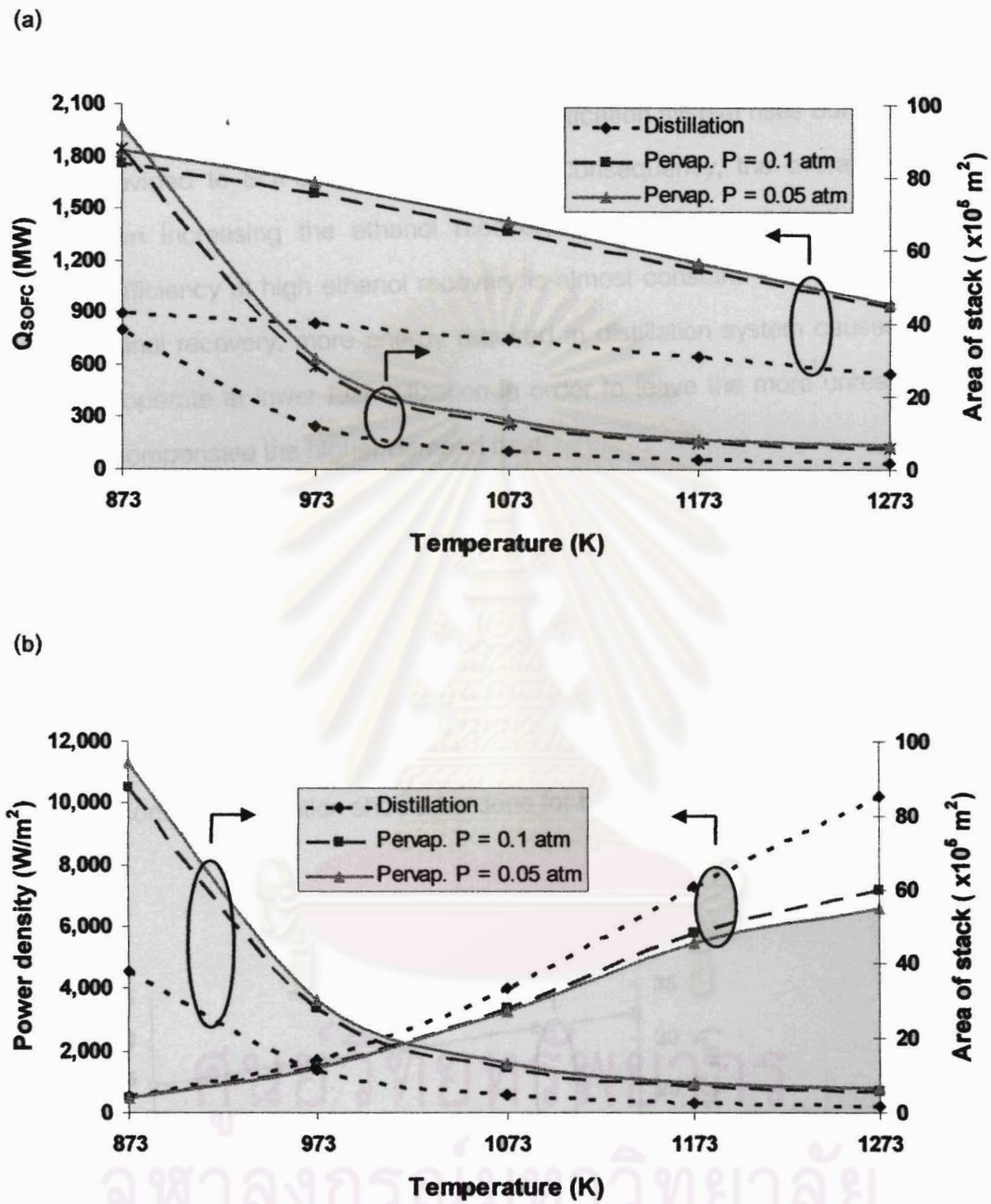


Figure 5.14 Effect of the operating temperature on (a) the heat of SOFC stack (Q_{SOFC}) and the area of SOFC stack and (b) the power density and the area of SOFC stack (Ethanol recovery = 80%, Voltage = 0.7 V)

For the effect of ethanol recovery, the overall electrical efficiency increase with the increasing of ethanol recovery as shown in Figure 5.15. Although at the higher ethanol recovery, the required energy for the purification system rises but the amount of ethanol provided to SOFC system increases. Consequently, the overall efficiency is higher when increasing the ethanol recovery. However, for distillation, the overall electrical efficiency at high ethanol recovery is almost constant. This is because at the higher ethanol recovery, more energy required in distillation system causes the SOFC system to operate at lower fuel utilization in order to leave the more unreacted fuel to burn and compensate the higher demand heat.

It can be seen that the SOFC system integrated with pervaporation unit provides higher electrical efficiency than that integrated with distillation column unit. Furthermore, the lowering pressure at the membrane permeation side offers slightly lower electrical efficiency than the other case. However, it should be noted that the area of SOFC stack in case of pervaporation is higher than that for distillation. Therefore, it is recommended that the economic evaluation should be done for both systems.

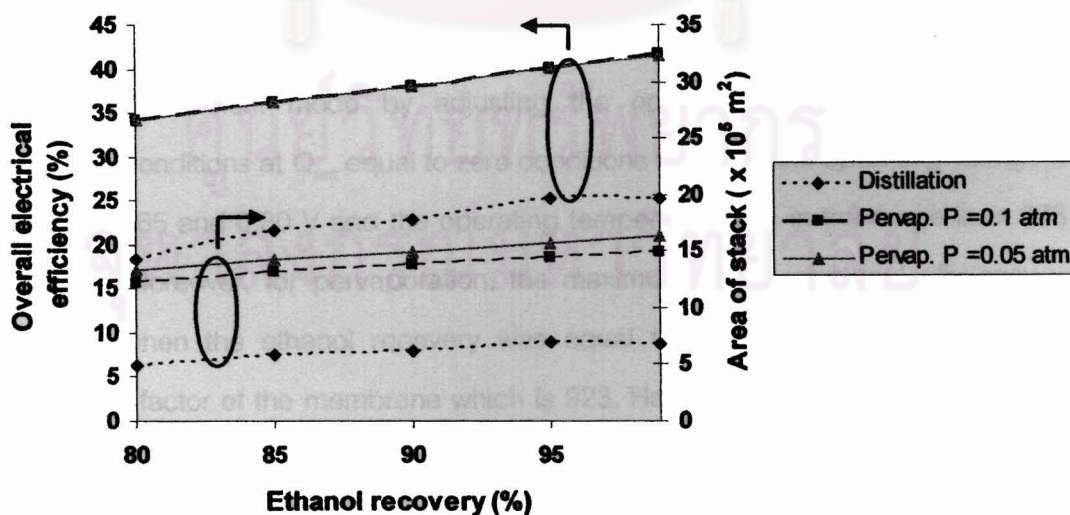


Figure 5.15 Effect of the ethanol recovery on the overall electrical efficiency and the area of SOFC stack (Voltage = 0.7 V, Temperature = 1073 K)

CHAPTER VI

CONCLUSIONS AND RECOMMENDATIONS

6.1 Conclusions

The SOFC system integrated with two different purification processes, i.e. distillation and pervaporation were studied. Bioethanol was used as a fuel for the system as it is an interesting renewable fuel that is non-toxic, easy for storage and transportation. In case of the purification process, it was found that the purification by pervaporation consumed less heat energy than that by distillation. However, the additional electrical power is required for the vacuum pump operation. For pervaporation process, the permeate pressure of 0.1 and 0.05 atm were investigated. The results indicated that the lowering pressure at the permeate side required less heat consumption and more electrical power consumption.

For the SOFC system integrated with the purification process, the influence of operating conditions such as voltage, temperature and ethanol recovery on the SOFC performances was presented. The result showed that the system can operate in an energy self-sufficient mode by adjusting the operating parameters. The optimal operating conditions at Q_{net} equal to zero conditions were that the operating voltage was between 0.65 and 0.80 V and the operating temperature was in the range from 973 to 1173 K. Moreover, for pervaporation, the maximum overall electrical efficiency was archived when the ethanol recovery was equal to 99% but it requires the higher separation factor of the membrane which is 923. However, the area of the SOFC stack also increased as the ethanol recovery increased. In case of distillation, the maximum overall electrical efficiency at high ethanol recovery operation was nearly constant due to the increasing of energy demand for the distillation unit hence the optimal ethanol recovery was 95%. It was found that the SOFC system integrated with pervaporation

process with the permeate pressure of 0.1 atm achieved the maximum overall electrical efficiency that was 41.6% at the voltage = 0.7 V, temperature = 1073 K, separation factor = 923 and ethanol recovery = 99%. It should be noted that the lowering pressure at the membrane permeation side offered no good effect on the overall electrical efficiency because the overall electrical efficiency reduced but more electrical power required. Therefore, in term of energy, pervaporation might be an alternative process for bioethanol purification.

6.2 Recommendations

6.2.1 Besides the overall efficiency of the SOFC system integrated with pervaporation process increased with the increasing of the ethanol recovery but the required area of the SOFC stack and the separation factor of membrane also increased. Therefore, the economic evaluation should be further investigated in order to ensure that this system provides high performance with the acceptable investment cost.

6.2.2 This research is assumed that the compositions of bioethanol contained only ethanol and water in order to simplify the calculations. Therefore, further study is recommended to investigate the effect of the real compositions of bioethanol. Since the membrane for pervaporation process is high sensitive with the compositions of the feed solution.

REFERENCES

- Appleby A.J. and Foulkes F.R., The Fuel Cell Handbook Malabar, Florida: Krieger Publishing, 1993.
- Arteaga L. E., Peralta L. M., Kafarov V., Casas Y. and Gonzales E., Bioethanol steam reforming for ecological syngas and electricity production using a fuel cell SOFC system. Chemical Engineering Journal 136 (2008): 256–266.
- Arteaga-Perez L. E., Casas Y., Peralta L. M., Kafarov V., Dewulf J. and Giunta P., An auto-sustainable solid oxide fuel cell system fueled by bio-ethanol Process simulation and heat exchanger network synthesis. Chemical Engineering Journal 150 (2009): 242–251.
- Atsawin Thongsukmak and Sirkar K.K., Pervaporation membranes highly selective for solvents present in fermentation broths. Journal of Membrane Science 302 (2007): 45–58.
- Aupretre F., Descorme C., Duprez D., Casanave D. and Uzio D., Ethanol steam reforming over $Mg_xNi_{1-x}Al_2O_3$ spinel oxide-supported Rh catalysts. Journal of Catalysis 233 (2005): 464–477.
- Chang C.L. and Chang M.S., Preparation of multi-layer silicone/PVDF composite membranes for pervaporation of ethanol aqueous solutions. Journal of Membrane Science 238 (2004): 117–122.
- Chen H., Li Y., Liu J. and Yang W., Preparation and pervaporation performance of high-quality silicalite-1 membranes. Sci China Ser B-Chem 50, 1 (2007): 70-74.
- Chen H., Li Y., Zhu G., Liu J. and Yang W., Synthesis and pervaporation performance of high-reproducibility silicalite-1 membranes. Chinese Science Bulletin 53, 22 (2008): 3505-3510.

- Fadeev A. G., Kelley S.S., McMillan J.D., Selinskaya Ya.A., Khotimsky V.S. and Volkov V.V., Effect of yeast fermentation by-products on poly[1-(trimethylsilyl)-1 propyne] pervaporative performance. Journal of Membrane Science 214 (2003): 229–238.
- Gu J., Shi X., Bai Y., Zhang H., Zhang L. and Huang H., Silicalite-Filled Polyether-block-amides Membranes for Recovering Ethanol from Aqueous Solution by Pervaporation. Chem. Eng. Technol. 32, 1 (2009): 155–160.
- Hao Y. and Goodwin D. G., Efficiency and fuel utilization of methane-powered single-chamber solid oxide fuel cells. Journal of Power Sources 183 (2008): 157–163.
- Kaneko T., Brouwer J. and Samuelsen G.S., Power and temperature control of fluctuating biomass gas fueled solid oxide fuel cell and micro gas turbine hybrid system. Journal of Power Sources 160 (2006): 316–325.
- Leng R., Wang C., Zhang C., Dai D. and Pu G., Life cycle inventory and energy analysis of cassava-based Fuel ethanol in China. Journal of Cleaner Production 16 (2008): 374–384.
- Lewandowska M. and Kujawski W., Ethanol production from lactose in a fermentation/pervaporation system. Journal of Food Engineering 79 (2007): 430–437.
- Lia L., Xiao Z., Tan S., Pu L. and Zhang Z., Composite PDMS membrane with high flux for the separation of organics from water by pervaporation. Journal of Membrane Science 243 (2004): 177–187.
- Lin X., Chen X., Kita H. and Okamoto K., Synthesis of Silicalite Tubular Membranes by *In Situ* Crystallization. AIChE Journal 49, 1 (2003): 237–247.
- Liu M., Peng R., Dong D., Gao J., Liu X. and Meng G. Direct liquid methanol-fueled solid oxide fuel cell. Journal of Power Sources 185 (2008): 188–192.
- Matsuda H., et al., Improvement of ethanol selectivity of silicalite membrane in pervaporation by silicone rubber coating. Journal of Membrane Science 210 (2002): 433–437.

- Ni M., Leung D. Y.C. and Leung M. K.H., Modeling of methane fed solid oxide fuel cells: Comparison between proton conducting electrolyte and oxygen ion conducting electrolyte. Journal of Power Sources 183 (2008): 133–142.
- Pakorn Piroonlerkgul, Suttichai Assabumrungrat, Navadol Laosiripojana and Adesina A.A., Selection of appropriate fuel processor for biogas-fuelled SOFC system. Chemical Engineering Journal 140 (2008): 341–351.
- Petruzzi L., Cocchi S. and Fineschi F., A global thermo-electrochemical model for SOFC systems design and engineering. Journal of Power Sources 118 (2003): 96–107
- Rabenstein G. and Hacker V., Hydrogen for fuel cells from ethanol by steam-reforming, partial-oxidation and combined auto-thermal reforming: A thermodynamic analysis. Journal of Power Sources 185 (2008): 1293–1304.
- Shiratori Y., Oshima T. and Sasaki K., Feasibility of direct-biogas SOFC. International journal of hydrogen energy 33 (2008): 6316-6321.
- Tao G., Armstrong T. and Virkar A., Intermediate temperature solid oxide fuel cell (IT-SOFC) research and development activities at MSRI. In: Nineteenth annual ACERC&ICES conference. Utah 2005
- Vane L. M., Review A review of pervaporation for product recovery from biomass fermentation processes. Journal of Chemical Technology and Biotechnology 80 (2005): 603-629.
- Vane L. M., Namboodiri V. V. and Bowen T. C., Hydrophobic zeolite–silicone rubber mixed matrix membranes for ethanol–water separation: Effect of zeolite and silicone component selection on pervaporation performance. Journal of Membrane Science 308 (2008): 230-241
- Verhoef A., Figoli A., Leen B., Bettens B., Drioli E. and Bruggen B. V., Performance of a nanofiltration membrane for removal of ethanol from aqueous solutions by pervaporation. Journal of Separation and Purification Technology 60 (2008): 54–63.

- Wassana Jamsak et al., Thermodynamic assessment of solid oxide fuel cell system integrated with bioethanol purification unit. Journal of Power Sources 174 (2007) 191–198.
- Wassana Jamsak et al., Design of a thermally integrated bioethanol-fueled solid oxide fuel cell system integrated with a distillation column. Journal of Power Sources 187 (2009): 190–203.
- Zhan X., Li J., Huang J. and Chen C., Enhanced Pervaporation Performance of Multi-layer PDMS/PVDF Composite Membrane for Ethanol Recovery from Aqueous Solution. Appl Biochem Biotechnol (2008): 1-11.
- Zhang L. and Yang W., Direct ammonia solid oxide fuel cell based on thin proton-conducting electrolyte. Journal of Power Sources 179 (2008): 92–95.
- Zhao F. and Virkar A. V., Dependence of polarization in anode-supported solid oxide fuel cells on various cell parameters. Journal of Power Sources 141 (2005): 79–95



ศูนย์วิทยทรัพยากร
จุฬาลงกรณ์มหาวิทยาลัย

APPENDIX A

THERMODYMIC DATA OF COMPONENTS

TABLE A1 Heat capacities of various components (C_p)

Components	$C_p/R = a + bT + cT^2 + dT^2 + eT^3$ [J/mol]				
	a	b (10^4)	c (10^{-6})	d (10^3)	e
CH ₄	1.702	90.800	-2.164	0.000	0.000
CO	3.376	5.570	0.000	-3.100	0.000
CO ₂	5.457	10.500	0.000	-1.160	0.000
H ₂ O	3.470	14.500	0.000	12.100	0.000
H ₂	3.249	4.220	0.000	8.300	0.000
N ₂	3.280	5.930	0.000	4.000	0.000
O ₂	3.639	5.060	0.000	-22.700	0.000
C	2.063	5.140	0.000	-1.060	0.000

TABLE A2 Heat of formation (H_f^0) and entropy (S^0) of various components at standard state (298 K, 1 atm)

Components	H_f^0 (kJ/mol)	S^0 (J/mol.K)
CH ₄	-74.52	186.27
CO	-110.53	197.70
CO ₂	-393.51	213.80
H ₂ O	-241.82	188.80
H ₂	0.00	130.70
N ₂	0.00	191.60
O ₂	0.00	205.20
C ₂ H ₆	-235.31	283.00

APPENDIX B

DETERMINING GIBBS ENERGY AND EQUILIBRIUM CONSTANT

B1. Determining Gibbs energy (G) at any temperature

Calculation by these equations:

$$G = H - TS \quad (\text{B1})$$

$$dG = dH - d(TS) \quad (\text{B2})$$

Take integration to the equation above:

$$\int dG = \int dH - \int d(TS) \quad (\text{B3})$$

$$G_T - G_{STD} = \int_{298}^T dH - \int_{298}^T d(TS) \quad (\text{B4})$$

where

$$H_f(T) = H_f^0 + \int_{298}^T C_p dT \quad (\text{B5})$$

$$S(T) = S^0 + \int_{298}^T \frac{C_p}{T} dT \quad (\text{B6})$$

B.2 Determining the equilibrium constant (K)

$$G_T = RT \ln K \quad (\text{B7})$$

Rearrange the equation:

$$K = \exp\left(-\frac{G_T}{RT}\right) \quad (\text{B8})$$

ศูนย์วิทยทรัพยากร
จุฬาลงกรณ์มหาวิทยาลัย

APPENDIX C**LIST OF PUBLICATION**

Issara Choedkiatsakul, Kanokporn Sintawarayan, Tanya Prawpipat, Apinan Soottitantawat, Wisitsree Wiyaratn, Worapon Kiatkittipong, Amornchai Arpornwichanop, Navadol Laosiripojana, Sumittra Charojrochkul and Suttichai Assabumrungrat, Performance assessment of SOFC system integrated with bio-ethanol production and purification process, Engineering Journal 13, 4 (2010) : 1-14.



ศูนย์วิทยทรัพยากร
จุฬาลงกรณ์มหาวิทยาลัย

VITAE

Miss Issara Choedkiatsakul was born in September 5, 1985 in Chumphon, Thailand. She received her Bachelor's Degree in Chemical Engineering (1st class honors), from the Department of Chemical Engineering, King Mongkut's Institute of Technology Ladkrabang in 2008. Afterward, she continued studying Master degree of Chemical Engineering, Chulalongkorn University since June 2008.



ศูนย์วิทยทรัพยากร
จุฬาลงกรณ์มหาวิทยาลัย